PERGAMON

Journal of South American Earth Sciences 13 (2000) 661–683

Journal of
South American
Earth Sciences

www.elsevier.nl/locate/jsames

The alkaline silica-saturated ultrapotassic magmatism of the Riacho do Pontal Fold Belt, NE Brazil: an example of syenite–granite Neoproterozoic association

J. Plá Cid[a,*], L.V.S. Nardi[a], H. Conceição[b], B. Bonin[c], E.F. Jardim de Sá[d]

[a]*Instituto de Geociências, Universidade Federal do Rio Grande do Sul, Av. Bento Gonçalves 9500, Porto Alegre RS 91509-900, Brazil*
[b]*CPGG/PPPG, Instituto de Geociências, Universidade Federal da Bahia, Rua Caetano Moura 123, Salvador BA 40210-350, Brazil*
[c]*LPV, Departement des Sciences de la Terre, Université Paris-Sud XI, Bât. 504, Paris -Orsay cx F-91504, France*
[d]*CCET/UFRN, Departamento de Geologia, Universidade Federal do Rio Grande do Norte, Campus Universitário de Lagoa Nova, Natal RN 59072-970, Brazil*

Accepted 30 April 2000

Abstract

The Neoproterozoic of northeastern Brazil was marked by the development of collisional fold belts, mainly surrounding the São Francisco Craton, and an associated widespread granitic magmatism. The Casa Nova (555 ± 10 Ma, $Sr_i = 0.7068$ and Engraçadinha syenites and granites, intrusive in the Riacho do Pontal Fold Belt, are related to the late stages of this collisional event. Melanocratic syenites, probably generated by magmatic-flow cumulate processes, and mesocratic and leucocratic syenites, representing magmatic liquids, are associated with granites, pegmatites, and syenite–granite dykes. Homogeneous or perthitic alkali feldspar, quartz, aegirine–augite, diopside, titanite, apatite, magnesian biotite, winchite–richterite, and magnetite are the dominant mineral phases. It is suggested that these magmas belong to an ultrapotassic silica-saturated alkaline series, defined on the basis of its alkaline, silica-saturated character and by a K_2O/Na_2O ratio of >3.0 — that is, intermediate. Major- and trace-element evolution is consistent with mineral fractionation processes, controlled by magmatic flow, and dominated by apatite–titanite–pyroxene in the less differentiated terms and by alkali feldspar in the more evolved. The source of primary magmas is a previously subduction-metasomatised mantle, probably with anomalous enrichment in LREE and LILE elements. Barite–ilmenite mineralisations are related to the more differentiated Engraçadinha granites.

Keywords: Ultrapotassic magmatism; Syenites; Geochemistry

1. Introduction

Since the 1970s, the São Francisco Craton of northeastern Brazil (SFC; Fig. 1A) and its marginal fold belts have been the object of works dealing with its definition, characterisation, and tectonic evolution (e.g. Almeida et al., 1977; Santos and Caldasso, 1978; Inda and Barbosa, 1978; Mascarenhas, 1979; Schobbenhaus et al., 1984; Figuerôa and Filho, 1990; Almeida et al., 1977; Barbosa and Dominguez, 1996; and references therein). The following orogenic cycles have been identified in the SFC (Wernick, 1981): Guriense (>3.0 Ga); Jequié (2.7 ± 0.1 Ga); Transamazônico (2.0 ± 0.2 Ga) and Brasiliano (1.0–0.52 Ga). Almeida et al. (1977) suggested a model of tectonic evolution for this region in which the cratonic structure, stable since the Mesoproterozoic, is surrounded by fold belts generated during the Brasiliano event. Caby and Arthaud (1987), Rocha (1991) and Almeida et al. (1977) have demonstrated that this event was locally active within the São Francisco Craton. The general structural pattern of the fold belts, transverse to the craton border (Fig. 1B), has been attributed to a series of collisions at the end of the Brasiliano event (Barbosa and Dominguez, 1996).

The magmatic suites discussed in this paper are intrusive in the Riacho do Pontal Fold Belt (RPFB, Fig. 1B), near the juncture of the states of Bahia, Pernambuco, and Piauí in NE Brazil. This fold belt is included in the Borborema Structural Province (Fig. 2), which is the largest such element in NE Brazil. The RPFB occupies the southwestern part of the central portion of this structural element (Fig. 2).

The northeastern portion of the Borborema Province, the Seridó Belt (Fig. 2), was structurally characterized by Jardim de Sá (1994), who identified high-K calc-alkaline or shoshonitic basic to intermediate rocks and alkaline and peraluminous granitoids with ages varying from 580 ± 30 Ma to 500–540 Ma. The younger magmatism is represented by peraluminous granitoids (Jardim de Sá,

* Corresponding author. Tel.: +55-51-316-6337; fax: +55-51-319-1811.
E-mail address: placid@if.ufrgs.br (J. Plá Cid).

0895-9811/00/$ - see front matter
PII: S0895-9811(00)00047-X

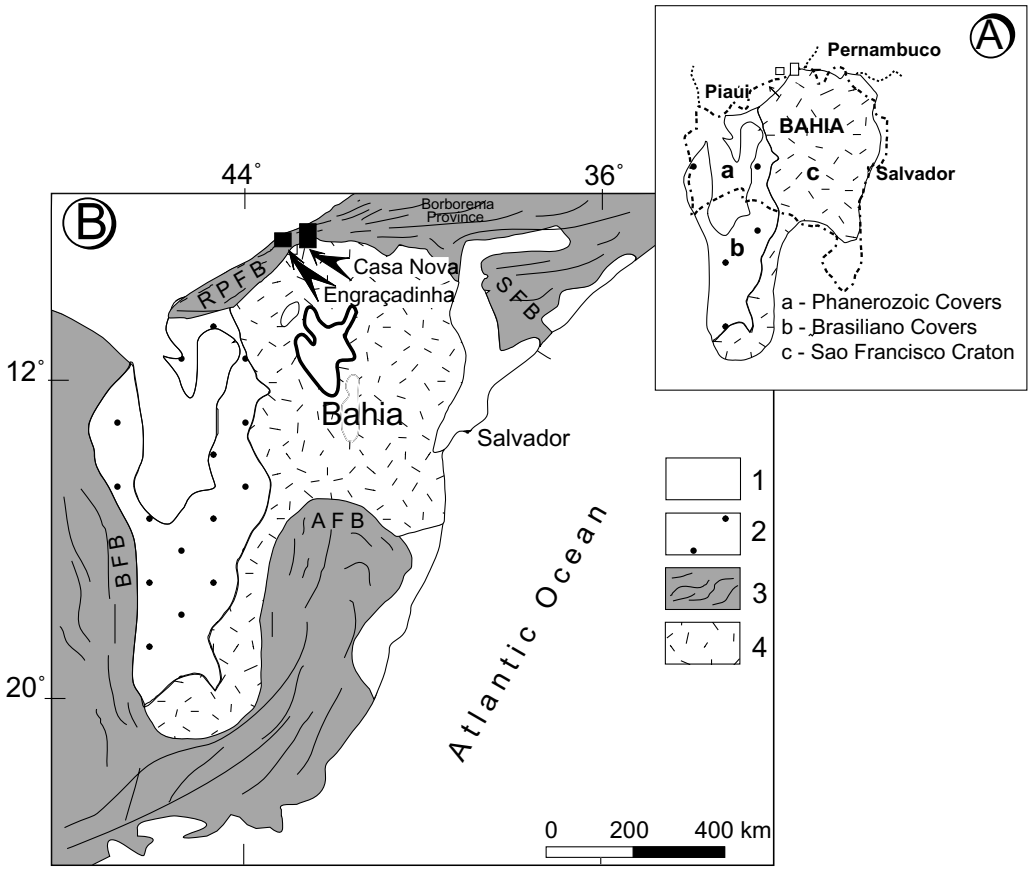

Fig. 1. (A) The São francisco craton within the state of bahia. (B) Main geological units of the são francisco craton, modified after Almeida et al. (1977): 1 = Phanerozoic covers; 2 = Neoproterozoic covers; 3 = Brasiliano fold belts; and 4 = craton terrains. RPFB = Brasiliano riacho do pontal and rio preto fold Belts; AFB = AraçuaÍ fold belt; SFB = Sergipano fold belt; BFB = BrasÍlia Fold Belt. Locations of syenite occurrences (Casa nova and engraçadinha complexes) denoted by solid rectangles.

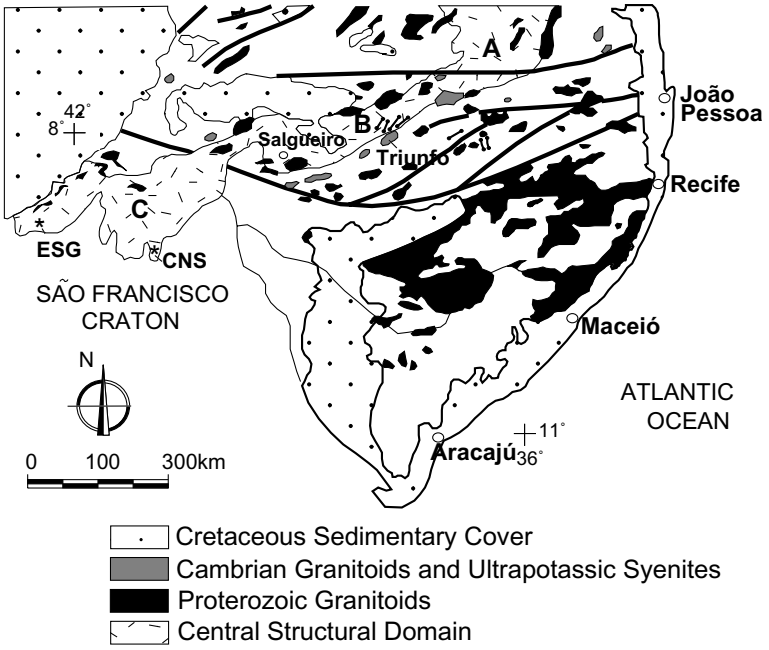

Fig. 2. Borborema province, its lithologies and structural domains (modified from Sial and Ferreira, 1988). The central structural domain (light grey): A, Seridó Fold Belt; B, Cachoeirinha–Salgueiro fold belt; C, Riacho do Pontal Fold Belt; ∗ESG = Engraçadinha syenites–granites; ∗CNS = Casa Nova syenites.

1994). The tectonic patterns, geochemical features, and Sr–Nd isotopes in basic to intermediate rocks of the Seridó Belt support the presence of a lithospheric mantle, enriched during a Paleoproterozoic subduction, in an arc-type tectonic setting (Jardim de Sá, 1994).

Granitoids with approximately the same geochemical affinities have been identified by Sial (1986) in the Cachoeirinha–Salgueiro Fold Belt within the central portion of the Borborema Province (Fig. 2). A Paleoproterozoic subduction zone has been proposed by Ferreira et al. (1994) to explain the distribution and geochemical affinities of Cachoeirinha–Salgueiro Brasiliano granitoids.

Jardim de Sá (1994) suggested that, in the Seridó Belt, the Brasiliano event is essentially marked by crustal block collisions under a transcurrent kinematic regime. According to this author, the northern part of the RPFB is a Mesoproterozoic terrain accreted to the cratonic margin during the Brasiliano collisional event. On the other hand, Leite (1997) demonstrated that the southwestern part of this fold belt is essentially a Paleoproterozoic terrain, with intensive sedimentation events during the Mesoproterozoic and major structural patterns originated by a frontal collision of crustal blocks during the Neoproterozoic.

2. Geological aspects of the Riacho do Pontal Fold Belt

The RPFB was originally defined by Brito Neves (1975) and later revised by Almeida et al. (1977). It includes greenschist to low-amphibolite grade metamorphic complexes (Silva, 1987), represented by the Casa Nova and Lagoa do Alegre metasedimentary rocks and magmatic units.

The Casa Nova Complex, which occurs over most of the area, encompasses carbonate-rich marbles, chlorite–muscovite, garnet–muscovite, and quartz–feldspathic schist and quartzite. It represents the host rocks of one syenitic association discussed in this paper. The age of the Casa Nova Complex is controversial. According to Bruni et al. (1974) and Schobbenhaus et al. (1984), this complex is Neoproterozoic; on the other hand, Inda and Barbosa (1978), Mascarenhas (1979) and Barbosa and Dominguez (1996) related it to the Paleoproterozoic Salgueiro Group.

The Lagoa do Alegre Complex, which crops out in the western portions of the RPFB, is Paleoproterozoic in age according to Barbosa and Dominguez (1996). This complex is composed of schists, paragneisses, quartzites, metabasic rocks, and iron-formations (Minadorzinho Unity), and metamafic/ultramafic rocks, on-formations, mica-schist, calc-silicates rocks and paragneisses (Macambira Unity).

Paleoproterozoic to Archean metamorphic units in the RPFB have been defined by Dalton de Souza et al. (1979), Figuerôa and Filho (1990), and many others. Dalton de Souza et al. (1979) defined a Metamorphic–Migmatitic Complex of Archean age, and an Early Proterozoic isotopic resetting. This metamorphic complex is well documented in the central and western parts of the RPFB. In the southern part of the RPFB, Figuerôa and Filho (1990) have defined the occurrence of Paleoproterozoic granitoids**,** represented by Sobrado-type granites and granodiorites, with a whole-rock Rb/Sr age of 2004 ± 107 Ma, $Sr_i = 0.735$ and a probable calc-alkaline affinity. The Neoproterozoic magmatism in this area is represented by Casa Nova syenites (CNS) (Rb–Sr age of 555 ± 10 Ma, $Sr_i = 0.7068$ Jardim de Sá, 1994), Engraçadinha syenites–granites (Dalton de Souza et al., 1979; Plá Cid et al., 1997a), and biotite–muscovite ± garnet granites (Dalton de Souza et al., 1979; Jardim de Sá, 1994), of anatectic origin and an Rb–Sr age of 539 ± 25 Ma (Figuerôa and Filho, 1990). Magmatic epidote-bearing granite intrusions occur in the eastern portion of the CNS (Fig. 3), or as enclaves engulfed by these syenites. Furthermore, Jardim de Sá (1994) has identified Neoproterozoic magmatism with high-K calc-alkaline or shoshonitic affinity in the northern part of the RPFB, close to the border of the Cachoeirinha–Salgueiro Fold Belt (Fig. 2). The Neoproterozoic associations studied are represented by the CNS and Engraçadinha syenites–granites.

3. Geological aspects of the syenites–granites

The syenitic and granitic suites studied are representative of the CNS and Engraçadinha syenites–granites (ESG, Plá Cid et al., 1997a,b). The CNS occurs in the north-eastern part of the RPFB (Fig. 3), whereas the ESG are located about 200 km to the northwest, in the State of Piauí, near the town of Bom Jardim (Fig. 4). Both suites are represented by small circular stocks, with deformation limited to narrow shear zones. This feature suggests a late- to post-Brasiliano emplacement of both suites, as already observed by Figuerôa and Filho (1990) and Dalton de Souza et al. (1979).

3.1. Casa Nova Syenites

A summary of the principal field characteristics of the CNS are given in Table 1. The CNS include two bodies, characterized by their positive relief, which contrasts with the flat morphology of the basement rocks. The eastern portion of the largest body is made up of epidote-bearing monzo- and syenogranite (Fig. 3). Preliminary petrographic observations and geochemical data point to a probable high-K calc-alkaline or shoshonitic signature for these granitoids, and the relation contacts with syenitic rocks suggest its older age.

The structural pattern is coherent with the late-tectonic emplacement of Casa Nova plutonism, confirmed by the Rb–Sr isochron. The roughly circular shape and structures of both bodies suggest that this plutonism was intrusive in the RPFB metamorphic terrains during the later phases of its stabilisation during the Brasiliano Cycle, post-dating the major deformational phases. Based on field and

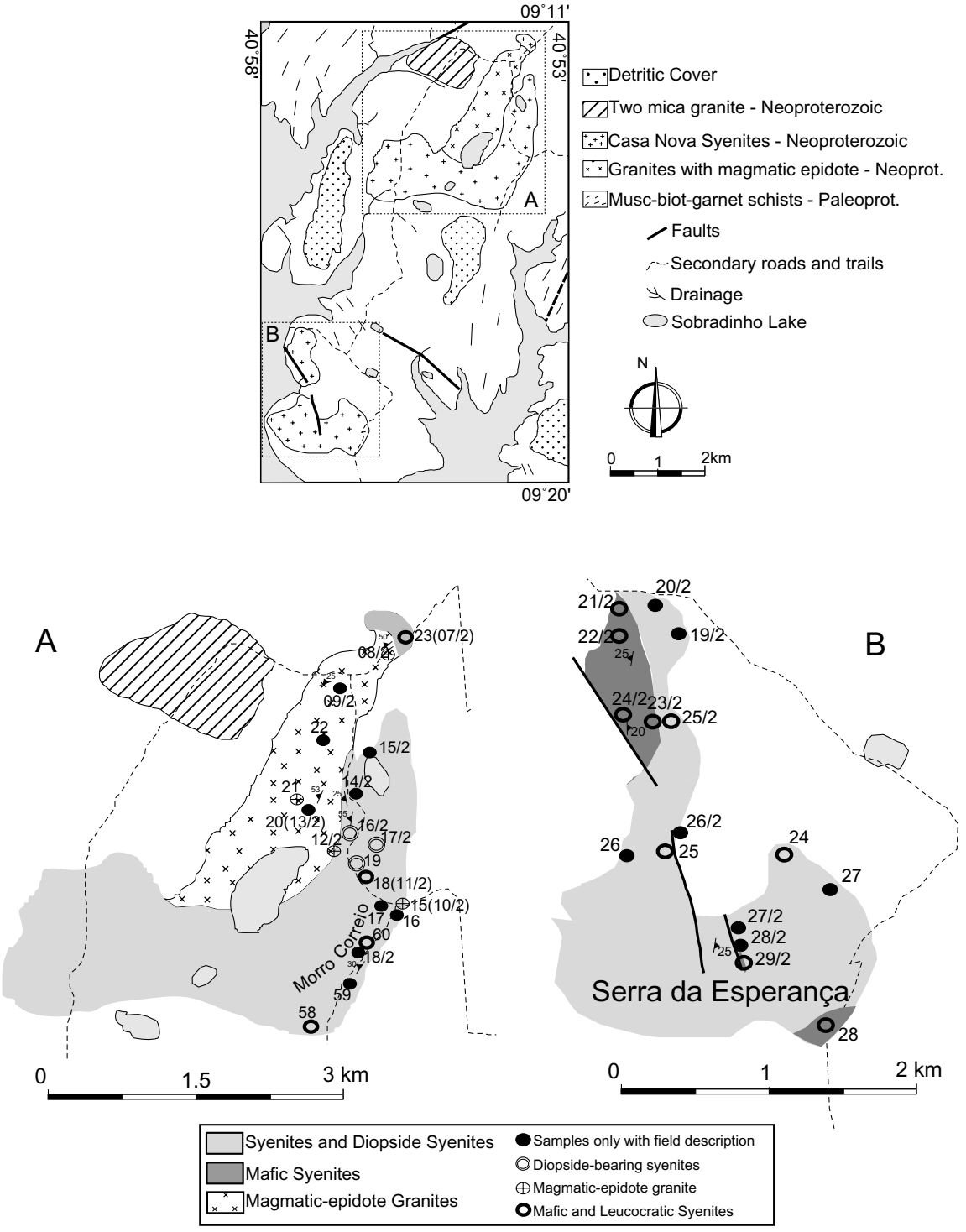

Fig. 3. Geological map of the Casa Nova ultrapotassic suite, showing sample locations; see Tables 4 and 5 for chemical analyses.

petrographic data, there are two different facies, identified as mafic and leucocratic syenites, and two dyke generations.

3.1.1. Mafic syenitic facies (MSF)

Mafic syenitic rocks occur in the topographically lowest portions, near Serra da Esperança (Fig. 3). This facies encompasses fine- to medium-grained rocks, normally with isotropic fabric, with local orientation. They are greenish-black in colour, with yellow punctuations of titanite. The modal proportions of mafic minerals, mainly aegirine–augite, can reach up to 60% (melanocratic syenites), with mean proportions around 35% (mesocratic syenites). Alkali feldspar occurs as anhedral to subhedral phenocrysts, arranged as parallel centimetre-size layers

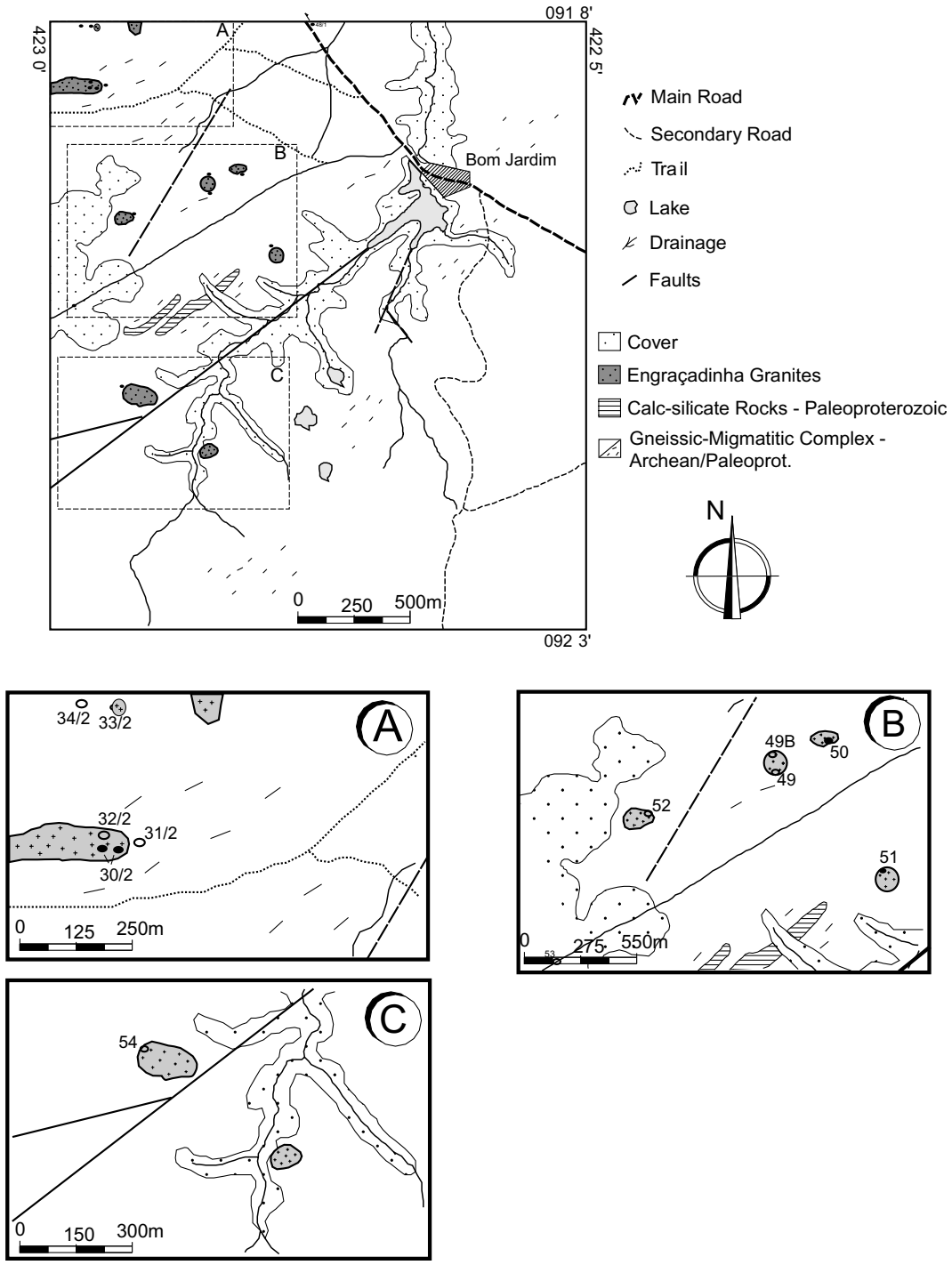

Fig. 4. Simplified geological map of the engraçadinha ultrapotassic suite, showing sample locations. Open circles indicate samples with chemical analyses, see Table 6.

produced by flow segregation during a ductile–brittle deformational stage. The orientation of these layers is coincident with the mafic syenite magmatic foliation.

Diopside-bearing mafic syenites occur close to the epidote-bearing granitoids (Fig. 3). They are medium-grained rocks, crosscut by the leucocratic syenites and syenitic–granitic dykes. Near the contact with leucocratic rocks, the diopside-bearing syenites are observed as decimetre-size enclaves (autholiths?) with irregular shape engulfed by the leucocratic rocks. They have preserved primary features, such as centimetre-size melanocratic lenses oriented parallel to the regional foliation, that could represent segregation due to magmatic flow, or mafic globules of the parental magma.

Table 1
Field characteristics of the Casa Nova and Engraçadinha suites

	Casa Nova Suite	Engraçadinha Suite
Form and Size	Two bodies, irregular to roughly circular, 16 km^2 and 6 km^2.	A dozen small circular stocks. < 0.1 km^2.
Host Rocks	Garnet–biotite–muscovite–schist: Casa Nova Complex.	Biotite–muscovite–gneiss: Metamorphic–Migmatitic Complex.
Contacts	Widespread occurrence of xenoliths of the Casa Nova Complex.	Gneissic rocks observed at the base of circular stocks.
Orientation	Magmatic foliation: alkali feldspar and pyroxene; cm-size shear zones. Both features are parallel to the regional orientation.	Weak alignment: acicular pyroxene and pyroxene-rich cm-size layers.
Magmatic Features	Banding of feldspar and feldspar + pyroxene layers. Decimeter-size autoliths of mafic-syenite in leucocratic-syenite.	Very homogeneous.

3.1.2. Leucocratic syenitic facies (LSF)

Leucocratic syenites represent most of the CNS suite. They are medium grey alkali feldspar syenites, with medium- to coarse-grained texture; feldspar and pyroxene reach up to 1.0 cm. Quartz can reach up to 10% in modal proportion in the most differentiated terms. The leucocratic syenites have an oriented fabric given by: (i) acicular pyroxene crystals and subhedral feldspars; (ii) centimetre-size bands, with up to 1 cm thick pyroxene-rich layers; (iii) rhythmically alternated leucocratic and mafic bands; and (iv) diopside-bearing syenite enclaves, with irregular or elliptic shape, and diffuse or more scarcely sharp contacts, reaching dimensions of 30 cm. These mafic autoliths present lobated, curved and sharp contacts, characterised by the absence of border-reactions, which suggest a synchronic crystallisation for both facies. Pegmatitic syenites occur near Serra da Esperança (Fig. 3) and are made up of euhedral alkali feldspar megacrysts with up to 20 cm in a coarse leucocratic matrix. These rocks represent the latest magmatic expression of the massif.

Basement-derived schist xenoliths frequently occur with disk shape (Plá Cid et al., 1997a), oriented along the magmatic flow. The well-preserved igneous structures attest that only the later deformational stages of Brasiliano Event controlled the crystallisation of the CNS, probably during a brittle–ductile stage.

3.1.3. Syenitic and granitic dykes

Two generations of fine-grained granitic dykes and syenitic pegmatites with large alkali feldspar and pyroxene phenocrysts crosscut the CNS.

The first dyke generation is made up of an extensive dyke swarm, with thickness varying from centimetre- to metre-size, that crosscuts the CNS with sharp and marked contacts. These dykes consist of fine-grained granite and pegmatite syenite, which sometimes occur together and form composite dykes; they are emplaced along parallel fractures. Normally, this generation is oriented from N120 to 150°, with dips varying from 25 to 70°/NE, and is generally coincident with the flow structure of the syenitic host rocks. Near the Serra da Esperança (Fig. 3), only pegmatite dykes are observed, with N170°-NS orientation, that crosscut the coarse grained syenites.

The second, younger, dyke generation is formed of compositionally similar but narrower dykes that are less abundant in volume. Their orientation is N20-30° with dips to the northwest. Near Serra da Esperança, this generation consists of alkali feldspar pegmatite, metre-size in thickness, with orientation of N40–70° — following the same regional structural control showed by the first dyke generation.

In both generations, the dykes are locally associated with fine-grained mafic rocks that may occur as interstitial masses inside of the syenitic pegmatite dykes.

4. Petrography

According to the nomenclature proposed by Streckeisen (1976), the mafic facies is composed of meso- and melanocratic alkali feldspar syenites. The composition of the leucocratic terms varies from alkali feldspar syenite to quartz alkali feldspar syenite (Fig. 3), with pyroxene modal concentrations generally under 15%. The dykes are alkali feldspar granite and alkali feldspar syenite. A summary of the mineralogical compositions of the RPFB alkaline silica-saturated ultrapotassic rocks is presented in Table 2.

The meso- and melanocratic syenites (MSF) are inequigranular, medium-grained rocks, basically aegirine–augite crystals of 2.5 mm and homogeneous alkali feldspar (Or >90%) of 1.5 mm. The magmatic foliation is mainly given by pyroxene, as observed in the melanocratic rocks, whereas in the mesocratic types an incipient banding formed by mafic and felsic mineral concentrations is typical. Aegirine–augite is the dominant modal constituent of melanocratic syenites, with about 60–70% in volume. Titanite, apatite, and occasionally amphibole are common accessory minerals in the meso- and melanocratic syenites, reaching, on average, modal contents of 2, 0.3, and 1%, respectively. In the melanocratic rocks, light blue euhedral amphibole is observed as inclusions or as intergrowths with aegirine–augite. This amphibole was classified according to its chemical composition as belonging to the richterite–winchite series (Table 2). According to experimental studies by Foley (1992), Mitchell (1995) and Konzett (1997), K-rich amphibole is a mineral phase usually crystallised

Table 2
Chemistry of the mineralogy from RPFB ultrapotassic rocks

	Casa Nova Suite				Engraçadinha Suite	
	Diopside Syenite	Mafic Facies	Leucocratic Facies	Granite Dykes	Syenites and Granites	Ba–Ti Mineralization
Pyroxene[a]	Diopside; Aeg–Aug (Ac ≈ 18%)	Aeg–Aug (Ac 21–36%)	Aeg–Aug (Ac 36–45%)	Aeg–Aug (Ac 51–61%)	Aeg–Aug (Ac 33–53%)	Aeg–Aug/Aeg (Ac 64–79%)
Amphiibole	not detected	Winchite/Richterite	not detected	Not detected	Mg–Riebeckite	not detected
Feldspar	not analysed	Or 96 (Ba 0.22–0.64%)	Or 96 (Ba 0.47–1.64%)	Or 96 (Ba 0.10–0.18%)	Or86–96 (Ba 0.71–1.53%)	not analysed
Apatite	not analysed	(SrO up to 8.21%) (Ce2O3 up to 1.3%)	(SrO up to 1.98%) (Ce2O3 up to 1.15%)	Not detected	(SrO up to 4.14%) (Ce2O3 up to 0.62%)	not analysed

[a] Ac — content of acmite molecule.

directly from ultrapotassic liquids, such as lamproites, or occurring in kimberlite xenoliths. Richterite, associated with phlogopite and Ti-bearing mineral phases, is thought to be present in the metasomatised mantle sources of ultrapotassic magmatism (Dawson and Smith, 1977; Erlank et al., 1987).

Some mafic syenite samples are exposed near the Morro do Correio (Fig. 3) and show particular petrographic features. They are inequigranular rocks, made up of anhedral perthitic alkali feldspar of ca. 1.0 mm, and diopside grains of the same size, engulfed in a fine- to medium-grained groundmass, consisting of microcline, albite, and accessory minerals. In the groundmass, the orientation of these rocks is marked by elongated concentrations of titanite + aegirine–augite ± apatite, and sometimes brown biotite + titanite ± apatite forming millimetre-size layers. The general characteristics of the main mineral phases of the diopside-bearing syenites are described in Table 3.

The major difference among the dominant facies of CNS is in the modal increase of alkali feldspar with interstitial quartz in the more differentiated syenites, and the occurrence of biotite in the diopside-bearing mafic syenite. The leucocratic facies (LSF) encompasses porphyritic rocks made up of alkali feldspar and aegirine–augite subhedral phenocrysts, with a fine- to medium-grained groundmass formed by quartz, alkali feldspar, pyroxene, titanite, and apatite. Centimetre-size globular aggregates of aegirine–augite**,** titanite, and apatite are frequent. These same mineral phases plus alkali feldspar constitute centimetre-size layers formed by magmatic flow. In these layers is observed acicular pyroxene included in alkali feldspar, indicating quenching of early crystallised pyroxene. The magmatic foliation is also marked by the orientation of phenocrysts. The characteristics of main mineral phases from leuco and mafic syenites are presented in Table 3.

Based upon textural evidence, the suggested crystallisation order for the CNS is shown in Fig. 5. The granite dykes are characterised by a fine-grained equigranular texture, interstitial quartz, and a decrease in the content of aegirine–augite as well as in apatite and titanite abundance relative to the syenitic facies. Fine-grained mafic syenitic dykes have microfractures filled with carbonate.

4.1. Engraçadinha syenites–granites (ESG)

The Engraçadinha syenites–granites (ESG) are represented by isolated hills with relief of 50 to 100 m. They are brown-reddish in colour, of fine-grain size, and slightly anisotropic due to acicular pyroxene orientation or to magmatic flow segregation of pyroxene centimetre-size layers. The ESG rocks generally present an homogeneous fabric with the absence of enclaves, and rare fine-grained granite dykes.

The Engraçadinha granitoids are inequigranular to porphyritic, medium-grained alkali feldspar granite, quartz alkali feldspar syenite, and alkali feldspar syenite, with alkali feldspar phenocrysts reaching up to 4.5 mm in size. The groundmass is composed of the association pyroxene–titanite–apatite, feldspar, and quartz. These rocks can present the magmatic-flow orientation of major constituents, and are made up of alkali feldspar, quartz, and pyroxene forming about 90–95% in volume. The accessory minerals are titanite, albite, zircon, apatite, opaque minerals, and blue amphibole. The primary difference between the syenites and the granites is the higher modal quartz and lower mafic content of the latter. Some features of the dominant mineralogy are described in Table 3.

4.2. Ba–Ti Mineralised granites

Barium–titanium mineralisations occur mainly in medium-grained equigranular granites, with strong anisotropy given by oriented quartz lenses and interstitial mafic bands, composed of aegirine–augite and aegirine, ilmenite and barite.

The alkali feldspar grains are anhedral to subhedral, often showing a albite–pericline twin. They are homogeneous grains, with a large amount of quartz inclusions and some aegirine growth along their cleavages.

Lensoid quartz masses, which surround microcline crystals, show wavy extinction and mosaic texture. Aegirine–barite–ilmenite paragenesis occurs in association with these felsic masses or filling micro-fractures.

Generally, aegirine and ilmenite are interstitial; the latter is sometimes euhedral and occurs along the border or filling fractures of pyroxenes**.** Barite shows the same relation with pyroxene. As suggested by textural evidence, ilmenite is formed after barite. The barite–ilmenite paragenesis may have a “metasomatic” origin, associated with the late magmatic stages, during aegirine crystallisation (Plá Cid et al., 1997a,b).

Blue euhedral amphibole occurs along the aegirine borders, as a product of reaction with late-stage fluids/melts. The crystallisation order is shown in Fig. 5.

The petrographic and mineralogical relations observed in both the Casa Nova and Engraçadinha suites are consistent with their co-magmatic origin.

5. Geochemistry

Whole-rock analyses (Tables 4–6) were performed at the Centro de Estudos em Petrologia at the Universidade Federal do Rio Grande do Sul in Brasil, at the Activation Laboratories in Ontario, Canada, and the Centre de Recherches Pétrographiques et Géochimiques (CRPG/CNRS), Vandoevres des Nancy in France.

Potassium-enriched rocks have been classified as shoshonitic or merely potassic, and ultrapotassic (Wilson, 1989). The parameters for their discrimination (e.g. Foley et al., 1987) are useful only to some restricted lithological groups and to basic and intermediate rocks. In order to classify this

Table 3
Main petrographic characteristics of the mineralogy from RPFB ultrapotassic suites

	Feldspars	Pyroxene	Other minerals
A. Diopside-bearing syenites			
Size	Phenocrysts ca. 1.0 mm	Diopside ca. > 1.0 mm. Aegirine–augite ca. < 0.5 mm	
Diagnostic characteristics	Perthitic phenocrysts. Subgrains and subsolvus albite + microcline in their borders	Diopside phenocrysts, zoned to aegirine–augite in the borders. Aegirine–augite as clots in the groundmass	Elongated concentrations of aegirine–augite–titanite–apatite, and biotite–apatite–titanite
Orientation	Subsolvus mineralogy		Elongated concentrations are oriented
Inclusions	Microcline include albite, aegirine–augite, and titanite	Both pyroxenes include biotite, opaque, and apatite	Poikilitic aegirine–augite include microcline, titanite, and albite (elongated concentrations)
Observations	Albite: mosaic texture and sharp contacts. The fractures of phenocrysts are filled by aeg.–aug.–titanite–apatite		
B. Mafic and leucocratic syenites			
	Alkali feldspar	Pyroxene	Other minerals
Diagnostic characteristics	Subhedral, albite–pericline twin. Homogeneous or thin-vein perthites	Euhedral, green to greenish brown colour, occurs in the groundmass or as round clots with titanite and apatite	Apatite — elongated, with ca. 0.5 mm.
Titanite — Euhedral and ca. 0.25 mm			
Orientation	Occasionally oriented	Oriented, mainly in groundmass of LSF	Both minerals in the groundmass
Inclusions	Acicular and anhedral aegirine–augite; subhedral to euhedral titanite; sometimes zircon and plagioclase in LSF	Titanite and apatite; more rarely zircon	Mutual inclusions among pyroxene, apatite, and titanite
Observations		Simultaneous crystallization with apatite and titanite	Late magmatic magnetite
C. Engraçadinha suite			
Diagnostic characteristics	Subhedral. Albite–pericline twins. Homogeneous or thin perthites	Interstitial grains of green aegirine–augite	Interstitial crystals or mm-size layers of albite and quartz
Orientation	Observed	Observed	Due to albite–quartz mm-size layers
Inclusions	Acicular and prismatic pyroxene, euhedral titanite, both sometimes along the cleavage; subhedral zircon and apatite	Mutual inclusions with titanite and apatite	
Observations	Local subgrains in the borders	Frequently associated with subhedral titanite and apatite	–

magmatism through major element composition, the TAS diagram was used (Le Maitre et al., 1989).

The TAS diagram for the rocks in this study is presented in Fig. 6. For rocks plotting in the silica-saturated and alkaline fields, three subgroups are identified: a) when $K_2O < (Na_2O — 2)$ wt%, they are considered 'sodic'; b) when $K_2O > (Na_2O — 2)$, and $1.0 < K_2O/Na_2O < 3.0$, they are classified as potassic or shoshonitic; and c) when $K_2O/Na_2O > 3.0$, they are considered here as belonging to the ultrapotassic silica-saturated alkaline series (Plá Cid et al., 1999a). This classification follows the recommendations of the IUGS (Le Maitre et al., 1989) and is complemented by the suggestions of Foley et al. (1987). Shoshonitic rocks are distinguished from high-K calc-alkaline rocks based on their alkaline character, plotting in the silica-saturated field of theTAS diagram, and from ultrapotassic rocks by their lower K_2O/Na_2O ratio. The three groups of ultrapotassic rocks recognised by Foley et al. (1987) plot generally in silica-undersaturated fields and, in addition to $K_2O/Na_2O > 2.0$, they must show $K_2O > 3$ wt% for terms with $MgO > 3$ wt%. These criteria are inadequate to classify more evolved intermediate and acid rocks, as noticed

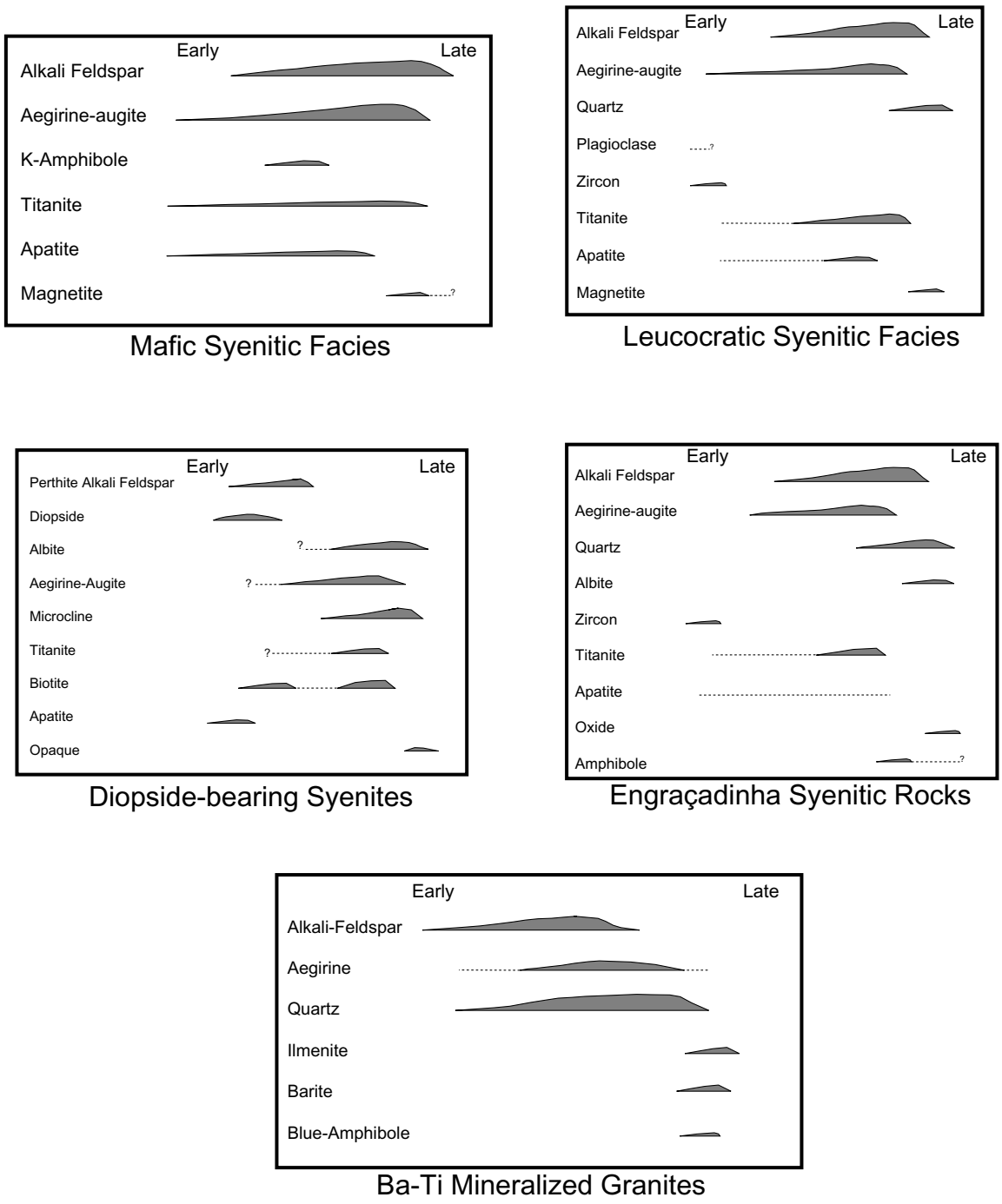

Fig. 5. The crystallization order of the casa nova and engraçadinha suites. The mafic syenites are made up of mesocratic and melanocratic facies. The engraçadinha suite encompasses syenites and quartz syenites.

previously by Ferreira (1991) in her study of syenitic rocks from northeastern Brazil. The Foley proposition is applicable only to basic and intermediate rocks. In the more evolved ultrapotassic liquids, MgO (<3.0 wt%) and K_2O/Na_2O (>3) contents reflect the intermediate to acid composition of the liquids. The aim of our suggestion is to discriminate silica-saturated to oversaturated alkaline ultrapotassic rocks from shoshonitic and from ultrapotassic undersaturated rocks (lamproites, kamafugites, and plagioleucitites).

Rocks plotting in the TAS rhyolitic or granitic field are classified mainly on the basis of cogenetic and less differentiated terms, since the relative and absolute proportions of alkalis may be strongly affected by fractionation.

As shown in Fig. 6, syenitic compositions are dominant in both suites studied, and granitic terms are subordinate. The more mafic Casa Nova rocks have less evolved composition, which reflects their high contents of modal pyroxene, whereas the fine-grained

Table 4
Whole-rock analyses of the Casa Nova suite (n.a. = not analyzed)

Sample	24A[a]	25[a]	58[a]	LE135/3[b]	LE135/3[b]	LE135/1[b]	LE135A[b]	LE159[b]	LE135B[b]	28A[c]	24B[a]	60B[a]
Facies	LSF	LSF	LSF	LSF	LSF	MSF	MSF	MSF	MSF	MSF	Dyke	Dyke
SiO_2	64.31	64.92	62.28	62.85	62.72	54.75	59.54	59.65	60.65	60.14	62.7	72.82
Al_2O_3	19.21	18.42	15.49	16.32	16.07	6.83	12.60	12.5	13.76	14.08	17.93	14.13
Fe_2O_3	1.03	1.06	2.26	2.37	2.87	13.10	7.60	7.50	5.83	4.28	1.37	1.41
FeO	0.12	0.24	0.84	n.a.	n.a.	n.a.	n.a.	n.a.	n.a.	n.a.	0.47	0.47
CaO	0.21	0.36	1.92	1.41	1.5	8.33	4.25	3.66	3.47	4.34	0.37	0.35
MgO	0.18	0.27	1.06	0.35	0.53	3.87	1.41	1.68	0.97	1.89	0.38	0.29
MnO	0.01	0.02	0.07	0.04	0.06	0.34	0.17	0.16	0.16	0.13	0.03	0.03
TiO_2	0.15	0.26	0.38	0.81	0.68	1.66	0.32	0.6	0.5	0.86	0.15	0.32
Na_2O	0.47	1.74	3.58	2.12	2.27	4.94	1.97	3.17	1.72	1.73	1.01	0.72
K_2O	13.14	11.72	11.12	12.13	11.8	4.66	10.33	9.44	11.32	10.79	12.86	9.65
P_2O_3	0.16	0.07	0.32	0.17	0.19	0.32	0.2	0.2	0.22	0.27	0.15	0.11
H_2Om	0.2	0.17	0.05	n.a.	n.a.	n.a.	n.a.	n.a.	n.a.	n.a.	0.18	0
LOI	0.17	0.33	0.44	0.56	0.47	0.7	0.72	0.49	0.51	0.63	0.34	0.44
Total	99.36	99.58	99.81	99.13	99.16	99.5	99.11	99.05	99.11	99.14	97.94	100.74
FeOT	1.05	1.19	2.87	2.13	2.58	11.79	6.84	6.75	5.25	3.85	1.70	1.74
Fe_2O_3T	1.16	1.33	3.19	2.37	2.87	13.10	7.60	7.50	5.83	4.28	1.89	1.93
NK/A	0.78	0.84	1.16	1.02	1.03	1.93	1.14	1.23	1.10	1.03	0.87	0.82
Cr	n.a.	n.a.	n.a.	n.a.	n.a.	n.a.	n.a.	n.a.	n.a.	71	n.a.	n.a.
Ni	18	17	20	9	10	83	40	29	30	33	18	17
V	33	52	142	136	143	592	323	331	240	127	70	145
Zr	76	42	114	47	46	172	227	538	177	204	189	87
Co	34	37	30	5	7	39	58	9	21	48.3	32	54
Cu	58	46	34	35	39	38	34	50	44	28.8	59	74
Ga	14	16	13	14	14	14	15	14	17	13.4	14	26
Nb	9	11	18	35	29	41	11	35	20	22	5	32
Pb	6	4	6	–	–	–	–	–	–	6.1	11	4
Zn	9	11	29	31	38	94	61	95	50	51.9	15	19
Rb	241	207	240	328	324	97	308	237	334	271	233	209
Sr	277	176	376	320	232	906	421	477	408	798	298	117
Ba	6009	4455	5466	4904	4892	1653	4908	4879	4812	10750	4898	1318
F	n.a.	100	290	n.a.	n.a.	n.a.	n.a.	n.a.	n.a.	n.a.	n.a.	150
Th	n.a.	5.7	11.6	5	5	23	7	55	5	12.3	n.a.	3.2
U	n.a.	0.5	2.2	n.a.	n.a.	n.a.	n.a.	n.a.	n.a.	1.5	n.a.	4.3
Y	n.a.	14	22	22	20	205	34	74	39	69	n.a.	16
La		22.10	41.20	38.16	34.18	280.36	38.69	97.06	35.11	86.76		26.60
Ce		64.80	109.1	127.54	114.98	494.26	107.76	186.63	104.93	199.40		81.70
Pr		7.04	11.40	n.a.	n.a.	n.a.	n.a.	n.a.	n.a.	33.90		8.43
Nd		33.40	54.4	75.69	59.54	276.55	64.45	123.30	62.01	155.40		40.70
Sm		6.60	10.60	16.59	13.59	55.97	14.79	26.12	15.02	34.85		8.30
Eu		1.87	3.02	4.32	3.63	12.85	3.83	7.02	3.91	10.40		2.18
Gd		5.30	8.40	10.82	9.45	45.95	11.04	20.70	11.80	25.16		6.50
Tb		0.70	1	n.a.	n.a.	n.a.	n.a.	n.a.	n.a.	3.23		0.80
Dy		2.80	4.20	5.45	4.45	32.25	6.12	12.95	6.47	14.85		3.50
Ho		0.40	0.60	n.a.	n.a.	n.a.	n.a.	n.a.	n.a.	2.11		0.50
Er		1.10	1.60	1.67	1.53	13.88	2.33	4.90	2.56	5.10		1.30
Tm		0.10	0.15	n.a.	n.a.	n.a.	n.a.	n.a.	n.a.	0.62		0.13
Yb		0.70	1	0.93	0.93	10.48	2.24	3.80	2.06	3.52		0.80
Lu		0.10	0.18	0.14	0.19	1.30	0.39	0.56	0.37	0.53		0.11

[a] Major elements and Nb, Co, Rb, Sr, Ba, Zr, Ga, Pb, Zn, and Ni were analysed by XRF at universidade federal do rio grande do sul. The other trace and all rare earth elements were analysed by ICP-MS at the activation laboratory, Ontario, Canada.
[b] Data obtained by Jardim de Sá (1994).
[c] Major elements were analyzed by emission-ICP, and trace and rare earth elements were analysed by ICP-MS, at centre de recherches pétrographiques et géochimiques, Université de Paris-Sud.

mafic dyke has a syenitic composition with slightly undersaturated character.

The K_2O/Na_2O ratio of the Casa Nova rocks varies from around 1.2 in diopside-bearing syenites and from 0.7 (cumulative syenites) to 6.2 in the mafic syenites and mafic dyke, increasing in concert with SiO_2 content, and reaching values between 3.1 and 27.9 in the syenites and granites. Extremely high values, such as 27, are present in the more leucocratic syenitic samples, due to feldspar accumulation. In the Engraçadinha suite, this ratio varies from 3.4 to 19.6.

Table 5
Whole-rock analyses of the Casa Nova suite (n.a. = not analyzed)

Sample	22A/2[a]	21B/2[a]	29/2[a]	22/2[a]	23/2[a]	16B/2[a]	07A/2[a]	17A/2[a]	21A/2[a]	23A/2[a]	24/2[a]	25/2[a]
Facies	Fine Dyke	MSF	MSF	MSF	MSF	MSF[b]	Granite	LSF	LSF	LSF	LSF	LSF
SiO_2	57.76	59.92	59.88	59.92	53.97	59.04	73.02	64.57	63.97	64.73	63.88	63.78
Al_2O_3	11.88	12.95	12.05	12.69	6.20	14.36	13.6	17.83	18.01	17.36	17.62	17.78
Fe_2O_3	9.21	7.61	7.93	7.47	13.47	5.06	0.87	1.17	1.18	1.38	1.55	1.58
FeO	n.a.	n.a.	n.a.	n.a.	n.a.	n.a.	n.a.	n.a.	n.a.	n.a.	n.a.	n.a.
CaO	5.09	3.73	4.49	3.87	9.15	5.58	0	0.22	0.28	0.07	0.56	0.82
MgO	0.91	1.50	2.45	1.79	4.44	1.81	0.09	0.02	0.06	0.33	0.18	0.22
MnO	0.19	0.13	0.15	0.14	0.36	0.13	0	0	0	0.02	0.03	0.02
TiO_2	0.52	0.47	0.30	0.18	1.80	0.42	0.06	0.06	0.17	0.13	0.28	0.26
Na_2O	3.49	3.02	4.24	3.31	5.30	4.90	1.55	1.33	1.47	1.94	2.06	3.16
K_2O	8.65	9.40	7.49	9.31	4.01	6.04	9.85	13.85	13.9	12.63	12.72	11.37
P_2O_3	0.17	0.04	0.07	0.06	0.35	0.86	0.09	< 0.01	< 0.01	0.17	0.11	0.03
LOI	1.62	0.72	0.58	0.63	0.51	0.43	0.46	0.51	0.62	0.85	0.74	0.59
Total	99.49	99.49	99.63	99.37	99.56	98.63	99.59	99.56	99.66	99.61	99.73	99.61
FeOT	8.29	6.85	7.14	6.72	12.12	4.55	0.78	1.05	1.06	1.24	1.39	1.42
NK/A	1.27	1.17	1.25	1.22	2.11	1.02	0.97	0.96	0.97	0.97	0.97	0.98
Cr	1.8	69.8	141	68	169	13.8	2.0	1.7	0.7	1.3	6.1	1.8
Ni	2.7	36	31.2	39.1	85.6	5.9	1.8	1.2	3.8	4.1	4.5	2.9
V	483	494	490	514	578	87	26	45	60	57	52	56
Zr	406	91	82	85	200	356	44	60	103	24	46	43
Co	73.7	62	83.4	75.7	109	65.2	78.5	53.7	93.6	83.5	64.5	70.5
Cu	10.9	3.3	6.5	11.7	16.2	26.7	3.6	5.6	2.9	6.9	5.6	5.3
Ga	21.5	24.4	18.8	21.8	14.7	17.8	20.4	22.5	22.1	19.1	16.6	15.7
Nb	25.7	14.8	4.1	2.4	36.7	14.2	5.6	8.1	9.6	4.7	9.6	11.3
Pb	6.22	3.17	5.43	1.38	5.81	30.10	10.70	3.40	2.07	2.76	2.38	7.25
Zn	76.2	52.7	58.3	49.7	121	91.4	13.9	20.2	14.8	17.8	19.9	19.3
Rb	208	197	152	219	86	118	278	314	294	273	257	213
Sr	788	439	537	334	861	2361	38	123	115	227	359	1314
Ba	2202	2937	1773	2366	1401	7512	2407	2974	4057	7018	6540	5720
Th	3.36	2.14	2.66	0.95	6.41	16.94	2.10	2.00	1.91	3.93	3.85	1.09
U	1.01	0.26	0.48	0.14	1.21	3.02	0.39	0.82	0.30	0.37	0.49	0.26
Y	11.8	10.3	19.2	24.2	161	29.8	2.2	5.1	11	24.6	46.9	32.6
Hf	16.6	2.9	2.4	2.6	7.2	7.6	1.5	1.3	1.9	0.6	1.3	1.3
Ta	4.30	2.11	0.38	0.45	3.09	1.06	0.70	0.74	0.95	0.68	0.87	1.10
Sn	20.1	13.5	10.1	12.4	21.1	2.4	1.6	1.9	2.5	2.2	2.8	2.6
La	32.07	15.60	28.37	24.57	238.60	60.99	5.99	15.65	18.15	48.94	67.24	52.18
Ce	83.96	69.75	68.21	82.54	478.50	142.90	15.28	27.49	63.79	95.18	109.80	107.40
Pr	10.92	10.16	9.61	12.68	71.32	18.71	1.93	4.24	9.32	14.35	17.82	13.86
Nd	44.47	42.18	37.07	56.10	284.7	74.52	7.13	15.77	39.88	58.48	75.12	56.01
Sm	9.01	9.86	7.55	13.30	57.49	15.39	1.34	2.95	8.29	11.72	14.12	11.25
Eu	2.74	2.72	2.16	3.62	12.13	5.34	0.77	1.29	2.51	4.15	4.71	4.00
Gd	5.69	5.47	5.46	9.04	44.27	12.26	1.01	2.15	5.01	9.01	12.18	8.65
Tb	0.75	0.71	0.79	1.22	6.43	1.47	0.14	0.25	0.67	1.12	1.67	1.17
Dy	3.23	3.09	3.87	5.39	33.88	6.50	0.55	1.21	2.93	5.67	8.43	5.56
Ho	0.43	0.39	0.64	0.86	5.95	0.93	0.10	0.18	0.40	0.91	1.43	0.90
Er	1.04	1.02	1.65	2.02	14.47	2.13	0.22	0.48	0.90	1.97	3.15	2.19
Tm	0.15	0.15	0.22	0.30	2.06	0.28	0.03	0.06	0.12	0.26	0.39	0.26
Yb	1.18	1.15	1.81	2.18	12.52	1.70	0.15	0.29	0.65	1.59	2.26	1.48
Lu	0.27	0.25	0.32	0.40	1.79	0.25	0.03	0.05	0.11	0.23	0.30	0.21

[a] Major elements were analyzed by emission-ICP, and trace and rare earth elements were analysed by ICP-MS, at centre de recherches pétrographiques et géochimiques, Université de Paris-Sud.
[b] Diopside-bearing syenite.

The CNS and ESG have peralkaline to metaluminous characters. The mafic syenites from the CNS and syenites from the ESG have agpaitic indices (Na + K/Al) ranging from 1.02 to 2.11 and from 1.01 to 1.03, respectively. The more evolved syenites in the Casa Nova suite and the Engraçadinha granites are dominantly metaluminous, with agpaitic indices ranging between 1.03 and 0.78 and 0.78 to 0.58, respectively. In both suites, this variation is reflected in the increase of sodic–calcic pyroxene together with decrease of alkali feldspar modal contents.

The suites studied are characterised by high concentrations of K_2O, Al_2O_3, Ba, Rb, and Sr (Plá Cid et al., 1997a). The K_2O contents reach values higher than 10 wt% in the CNS and around 9.7 wt% in the ESG. In

Table 6
Whole-rock analyses of the Engraçadinha suite (data obtained by Jardim de Sá (1994). n.a. = not analyzed)

Sample	31/2[a]	32/2[a]	33/2[a]	34/2[a]	52[b]	53[b]	49[b]	49B[b]	54[b]
Suite	ESG	ESG	ESG	ESG	ESG	ESG	Ba–Ti rocks	Ba–Ti rocks	Partially metasom.
SiO_2	67.36	66.9	64.04	64.76	71.93	67.21	75.37	83.30	79.48
Al_2O_3	14.66	14.8	14.56	14.82	17.47	15.97	7.22	6.55	7.50
Fe_2O_3	2.55	2.59	4.12	3.62	1	3.22	5.68	5.24	4.75
FeO	0	0	0	0	0.58	0.68	1.08	0.87	0.99
CaO	1.25	0.78	2.34	1.01	0.11	0.88	0.14	0.02	0.75
MgO	0.32	0.21	0.59	0.29	0.28	0.48	0.40	0.14	0.22
MnO	0.05	0.06	0.1	0.06	0.02	0.06	0.10	0.14	0.10
TiO_2	0.19	0.19	0.41	0.42	0.20	0.42	1.17	1.37	0.11
Na_2O	2.73	2.48	2.67	1.63	1.46	0.50	1.86	0.43	1.49
K_2O	9.47	10.07	9.81	11.64	7.20	9.83	5.12	3.94	3.84
P_2O_3	0.09	0.11	0.15	0.13	0.06	0.08	0.03	0.02	0.01
LOI	0.44	0.52	0.61	0.64	0.54	0.51	0.79	0.80	0.49
Total	99.11	98.71	99.40	99.02	100.94	99.90	99.07	102.94	99.78
FeOT	2.29	2.33	3.71	3.26	1.48	3.58	6.19	5.58	5.26
NK/A	1.01	1.01	1.03	1.03	0.58	0.72	1.19	0.76	0.88
Cr	2.5	1.7	9.7	n. a.	n. a.	n. a.	n. a.	n. a.	n. a.
Ni	3.5	1.7	6.0	1.9	19	17	14	15	14
V	36.9	39.7	61	56.7	23	91	64	47	19
Zr	158	144	300	144	117	142	605	735	249
Co	73.2	68.4	70.3	71.9	58	84	91	106	129
Cu	3.4	3.6	7.8	5.6	58	37	40	63	46
Ga	16.8	16.7	17.9	17	16	14	19	15	15
Nb	7.7	7.8	10.8	7.6	15	12	52	31	12
Pb	24.7	15.4	35.6	52.2	13	5	9	17	29
Zn	46.4	44.5	65.3	51.8	13	30	53	63	79
Rb	264.3	271.8	275	323.5	265	282	143	149	176
Sr	463	475	885	413	224	152	355	365	397
Ba	4846	5403	7800	9050	5233	5613	>10000	> 10000	2953
F	n. a.	n. a.	n. a.	n. a.	100	100	100	100	180
Th	10.48	9.82	15.16	21.14	9	8.33	40.47	99.89	29.35
Y	12.7	15.8	33	18.3	43	72	24	38	21
Hf	3.67	3.41	6.29	3.94	n. a.	n. a.	n. a.	n. a.	n. a.
Ta	0.952	1	1.17	1.04	n. a.	n. a.	n. a.	n. a.	n. a.
Sn	2.41	2.42	2.71	2.78	n. a.	n. a.	n. a.	n. a.	n. a.
La	20.49	26.49	40.61	56.34	91.80	66.60	62.10	103.20	21.90
Ce	42.18	49.40	95.63	98.93	200.30	132.90	94.40	158	32.10
Pr	5.07	6.52	12.15	10.45	20.09	19.47	6.81	10.96	2.87
Nd	19.58	24.22	48.77	36.71	87.70	92	24.90	38.20	10.60
Sm	4.09	4.77	9.99	6.88	15.40	17.60	3.90	5.90	2
Eu	2.06	2.4	4.19	3.54	3.46	4.44	1.69	2.09	0.67
Gd	2.94	3.76	7.42	5.27	13.40	15.40	4	6.20	2.50
Tb	0.43	0.50	1.07	0.70	1.80	2.20	0.60	0.90	0.40
Dy	2.15	2.80	6.03	3.76	8.40	11.40	3.50	5.30	2.70
Ho	0.40	0.50	1.09	0.71	1.40	2	0.80	1.10	0.60
Er	1.02	1.30	2.81	1.73	3.90	6	3.10	3.90	1.90
Tm	0.16	0.19	0.45	0.28	0.41	0.62	0.49	0.53	0.28
Yb	1.09	1.22	2.69	1.64	2.80	4	4.80	4.50	2.50
Lu	0.16	0.18	0.38	0.25	0.39	0.66	0.96	0.80	0.51

[a] Major elements were analyzed by emission-ICP, and trace and rare earth elements were analysed by ICP-MS, at centre de recherches pétrographiques et géochimiques, Université de Paris-Sud.
[b] Major elements and Nb, Co, Rb, Sr, Ba, Zr, Ga, Pb, Zn, and Ni were analysed by XRF at universidade federal do rio grande do sul. The other trace and all rare earth elements were analysed by ICP-MS at the Activation Laboratory, Ontario, Canada.

some cases, the high concentrations of these elements may reflect alkali feldspar cumulative processes. The fine-grained granitic dykes in the CNS, with 9.65% of K_2O (Table 4, sample 60B), and the fine-grained equigranular texture in the ESG, without textural evidence of cumulative processes, indicate that the K-enriched character is a magmatic feature. Furthermore, the calcic–pyroxene cores rimmed by aegirine–augite, which formed under liquidus conditions, suggest a continuous magmatic evolution from diopside-bearing to leucocratic syenites. Magmatic-flow cumulative processes involving the early crystallised phases is admitted for the generation of some mafic enriched

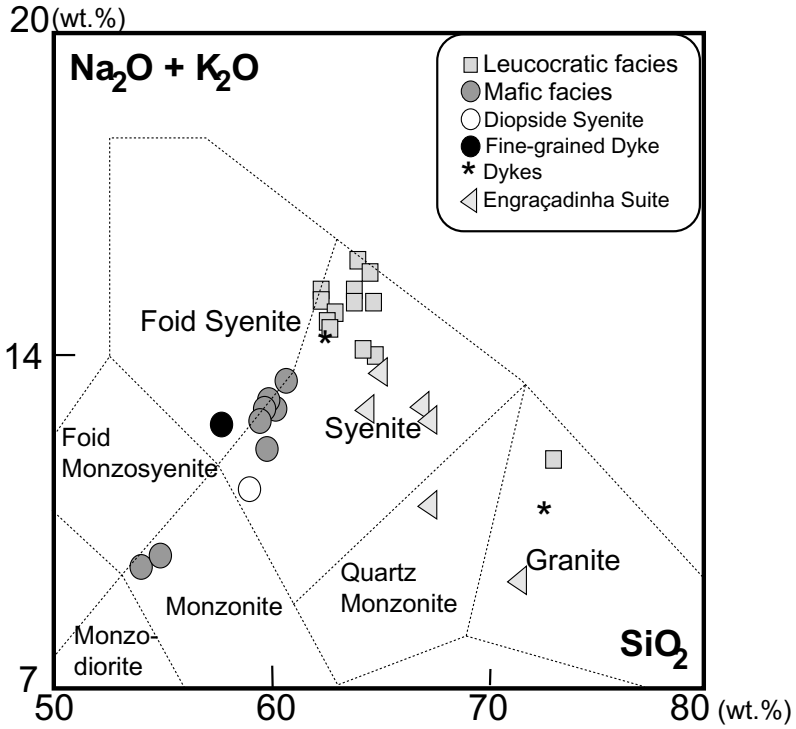

Fig. 6. Total alkali vs. silica (TAS) diagram (after Le Maitre et al., 1989), with chemical classification and nomenclature of plutonic rocks (from Middlemost, 1994).

layers such as those represented by samples 23/2, and LE-135/1, with $K_2O/Na_2O < 2$ and high pyroxene modal contents.

The most important features are: (i) a K_2O/Na_2O ratio that varies from 0.76 to 27.95 in the CNS and from 3.47 to 19.66 in the ESG; and (ii) K_2O contents that are higher than 3 wt% (Table 4). The MgO content is frequently lower than 3%, except for the more mafic syenites, samples LE-135/1 and 23/2 (Table 4), whose SiO_2 contents are comparable to the rocks referred by Foley et al. (1987). MgO contents decrease with magmatic differentiation, to less than 1% in the leucocratic syenites, with SiO_2 content about 64% in the syenitic–granitic dykes as well as in the Engraçadinha suite.

The low TiO_2 contents in the less differentiated terms suggest that the Casa Nova and Engraçadinha suites are probably related to sources typical of a collisional setting (Fig. 7), as suggested by Foley et al. (1987) for ultrapotassic Group III. The low TiO_2 contents of less evolved syenites, mainly in the Casa Nova suite, are related to a source signature, although in the more evolved terms the titanite fractionation promoted a decrease in TiO_2 contents (Fig. 7).

Shoshonitic and ultrapotassic saturated to oversaturated rocks, some of them with petrographic and geochemical characteristics comparable to the Casa Nova and Engraçadinha suites, have been described in southeastern Papua New Guinea (Smith, 1972), in southwestern Nigeria (Oyawoye, 1976), in syenites from Scotland (Thompson and Fowler, 1986), in syenitic dykes from Sinkiang Province, China (Pognante, 1990), in the Greenville Province, Canada (Corriveau et al., 1990), in the Little Murun ultrapotassic complex of the Aldan Shield, Russia (Mitchell and Vladykin, 1996), in the Cléricy Archean ultrapotassic syenite pluton in southern Abitibi, Canada (Laflèche et al., 1991), in syenites from western Africa (Laval and Hottin, 1992), and in the syenitic Paleoproterozoic province of Bahia, northeastern Brazil (Conceiçã et al., 1989, 1994; Conceiçã, 1990; Rosa, 1994). The Brasiliano belts in northeastern Brazil have several syenite–granite occurrences (Fig. 2) with comparable composition

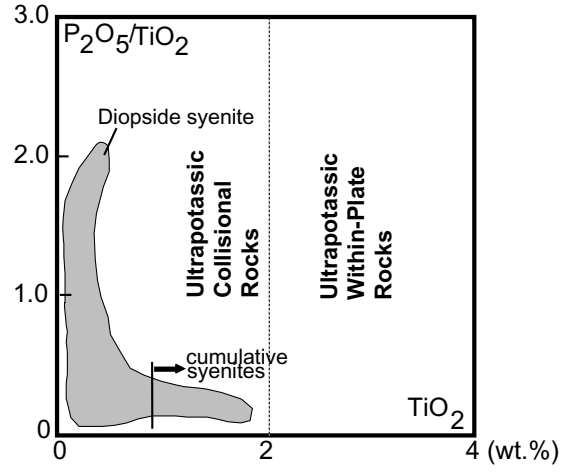

Fig. 7. P_2O_5 vs. TiO_2 diagram (after Foley et al., 1987) to discriminate between ultrapotassic rocks generated in orogenic and within-plate settings.

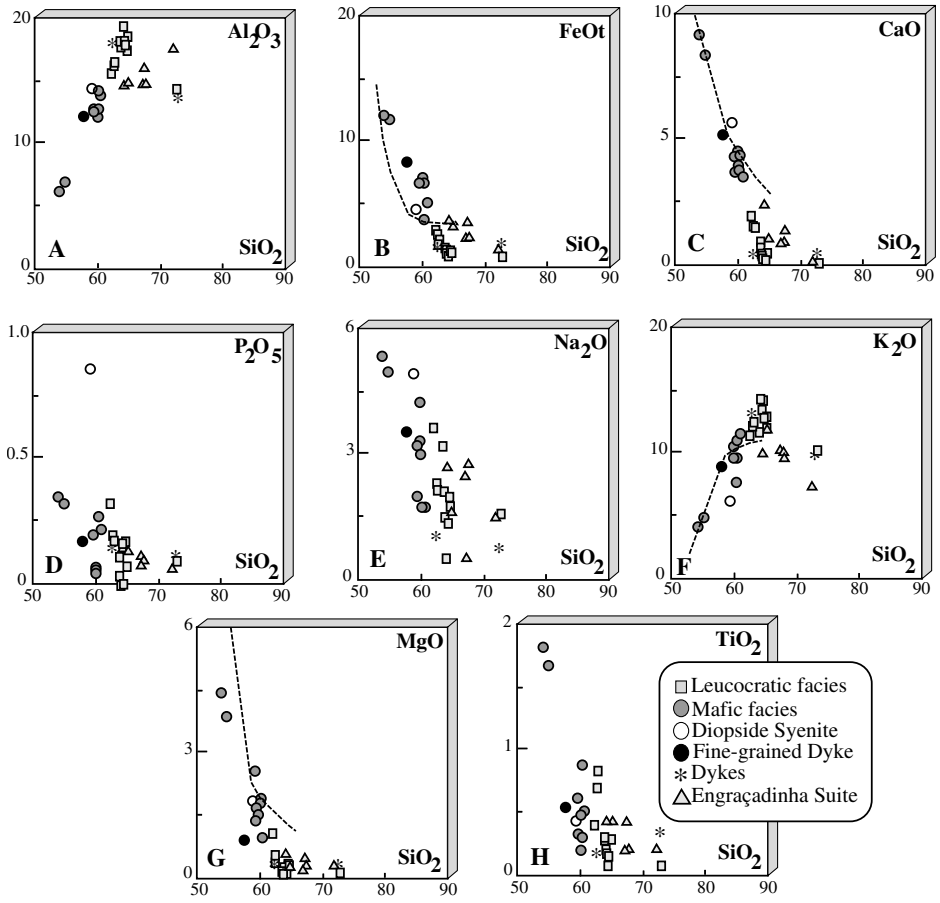

Fig. 8. Harker diagrams (in wt%) of the alkaline ultrapotassic rocks from the RPFB, and some evolutionary trends from the triunfo syenite (dashed line).

(Plá Cid et al., 1997a,b). They are oriented along NE–SW trends for hundreds of kilometres, and in the so-called syenitoid-alignment within the Cachoeirinha–Salgueiro Fold Belt (Fig. 2). They are represented by the Triunfo syenite (Ferreira, 1991; Ferreira et al., 1994), the ultrapotassic dykes of the Terra Nova pluton, and Serra do Livramento syenites (Da Silva Filho et al., 1987, 1993). Among all of these K-rich associations, the magmatism in the Cachoeirinha–Salgueiro Fold Belt, the Little Murun complex, the Clericy pluton, and syenites from western Africa present mineralogies and geochemical signatures comparable to RPFB ultrapotassic suites.

5.1. Major elements

The major element compositions of CNS and ESG were plotted in Harker-type variation diagrams (Fig. 8); the SiO_2 contents show a larger range in the CNS (53.97–73.02%) than in the ESG (64.04–71.93%).

Both suites present high concentrations of Al_2O_3 and K_2O; additionally, the mafic syenites present high contents of P_2O_5 (Fig. 8). Al and K show an incompatible behaviour, with strong enrichment in the LSF, whereas in the Engraçadinha suite they become compatible; that may be ascribed to alkali feldspar fractionation during the evolution to more evolved compositions (Fig. 8). The incompatible behaviour of Al and K probably reflects generation of the more mafic syenites through cumulative processes involving mainly pyroxene and controlled by flow mineral segregation.

CaO, MgO, FeOt, Fe_2O_3, and even Na_2O show compatible behaviour that is attributed to calcic–sodic pyroxene fractionation. TiO_2 and P_2O_5 present irregular behaviour, although generally the mafic syenites are richer in these elements as a reflection of the early crystallisation of titanite and apatite. The melanocratic syenites have extremely high contents of TiO_2 and P_2O_5, suggesting that apatite and titanite in these rocks are cumulative phases.

The Engraçadinha granites and syenites present major element distribution patterns that strongly indicate fractionation of pyroxene, titanite, and apatite. The major element composition of the RPFB alkaline silica-saturated ultrapotassic rocks indicates the importance of alkali feldspar and pyroxene flow segregation during magmatic crystallisation.

Fig. 8 illustrates the evolutionary trends of the Triunfo syenite, that shows compositions similar to those of the RPFB alkaline silica-saturated ultrapotassic rocks. The positive correlation observed for Al_2O_3 and K_2O, and the negative correlation for FeOt, CaO, MgO, MnO, TiO_2 and P_2O_5 vs. SiO_2 show the similarity of their magmatic

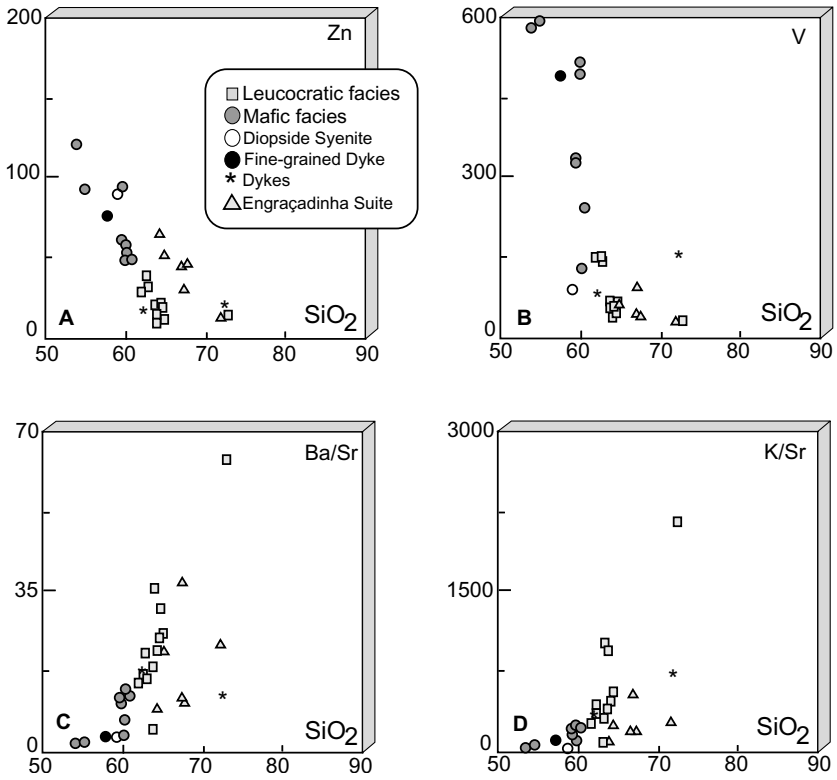

Fig. 9. Trace element variations in the RPFB alkaline silica-saturated ultrapotassic suites.

evolution. The principal differences between the RPFB magmatism and the Cachoeirinha–Salgueiro Fold Belt intrusions are the higher Al_2O_3 and K_2O and the lower FeOt and CaO contents in the former.

5.2. Trace elements

The trace element patterns in the Casa Nova and Engraçadinha suites are characterised by high values of Ba and medium to high values of Rb and Sr; Rb/Sr ratios are close to 1 in the Casa Nova syenitic facies and lower in the Engraçadinha rocks, mainly due to higher Sr contents. This ratio decreases sharply in the mafic syenites, also due to the Sr increase up to 2361 ppm in the diopside-bearing syenite (sample 16B/2, Table 5). The Sr increase in the less differentiated terms of both suites may be attributed to the increase in the modal content of apatite, which can contain up to 8.21 wt% of SrO (Table 2). The decrease of Rb and Ba contents in the mafic facies is explained by the low partition coefficients of these elements in the mafic cumulative phases. The same features were also observed in the Engraçadinha rocks. Cr, Ni, and Co show the highest concentrations in the melanocratic syenites, reflecting the high pyroxene modal content.

The fine-grained mafic dyke (sample 11A) and the diopside-bearing syenite (16B/2) have V, Zn, K/Sr, and Ba/Sr values intermediate between melano- and mesocratic-syenites (Fig. 9). These patterns also indicate that melanocratic syenites can represent pyroxene–syenite cumulates, as suggested by the trends observed in the Harker diagrams (Fig. 8).

The trace element distribution diagrams of both suites (Fig. 10), normalised to the values of chondrites (Thompson et al., 1982), show a negative slope and strong negative anomalies of Th, Nb, Ta, P, and Ti, and the more differentiated Engraçadinha granites overlap the leucocratic syenites of the CNS. P anomalies reflect the fractionation of apatite during differentiation. A negative Sr anomaly is absent in the less evolved rocks of the ESG, which are richer in P_2O_5 than more differentiated syenites and granites of this suite. This feature reflects the early crystallisation of Sr-rich apatite (Fig. 5).

The diopside-bearing syenites, considered to be the less evolved liquid of the CNS, show a significantly different pattern — lacking Th, P, and Sr anomalies, suggesting a magmatic source enriched in these elements. Early crystallisation of apatite in these syenites (Plá Cid et al., 1997b) explains the P and Sr negative anomalies in the more evolved facies.

The melanocratic syenites are enriched in most elements, except Rb and K, that could be explained by their origin through cumulative processes involving pyroxene, apatite, and titanite. Their negative Sr and P anomalies are due to the relative enrichment of REE that is ascribed to the titanite and apatite role as major carriers of REE in these syenites.

The negative Ti and Nb anomalies are ascribed by Foley and Wheller (1990) to the presence of Fe–Ti oxides among

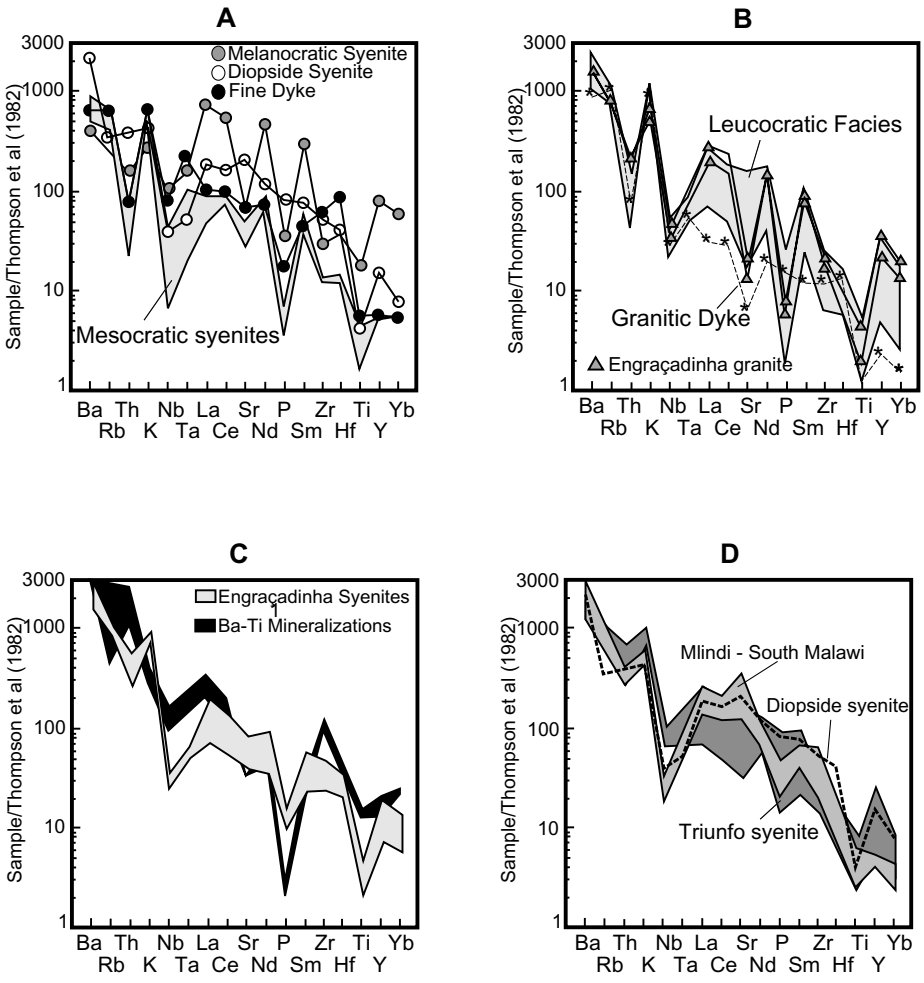

Fig. 10. Spidergrams normalised according to the chondritic values of Thompson et al. (1982). Ta and Hf contents from engraçadinha granites, Ba–Ti-mineralised granites, as well as the syenites from triunfo and africa were not reported.

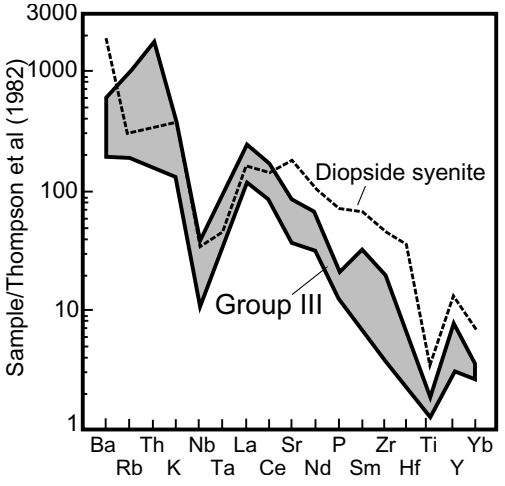

Fig. 11. Spidergram normalised according to the chondritic values of thompson et al. (1982) of the ultrapotassic group III (from Foley et al., 1987) and diopside-bearing syenite.

fractionated *liquidus* phases or among residual mantle phases. Pearce (1983) and Wilson (1989) ascribed the Ti, Nb, and Ta troughs displayed in spidergrams of potassic magmas to their generation from a subduction-modified mantle.

Fig. 11 illustrates that RPFB ultrapotassic suites have negative Ti–Ta–Nb anomalies similar to those observed in the ultrapotassic Group III of Foley et al. (1987), suggesting the probable genetic relation of this magmatism to an enriched-mantle source previously modified in a subduction setting. This hypothesis was also suggested by Ferreira (1991) for the ultrapotassic magmatism in the Cachoerinha–Salgueiro Fold Belt.

Ultrapotassic syenitic magmatism associated with collisional settings is usually related to previously subduction-modified sources as discussed by Thompson and Fowler (1986), Corriveau et al. (1990) and Ferreira et al. (1994). The ultrapotassic rocks of the RPFB have trace element patterns comparable to those of the pyroxenite–syenite association in Mlindi, Malawi (Laval and Hottin, 1992) and the Triunfo syenite (Ferreira, 1991) in the

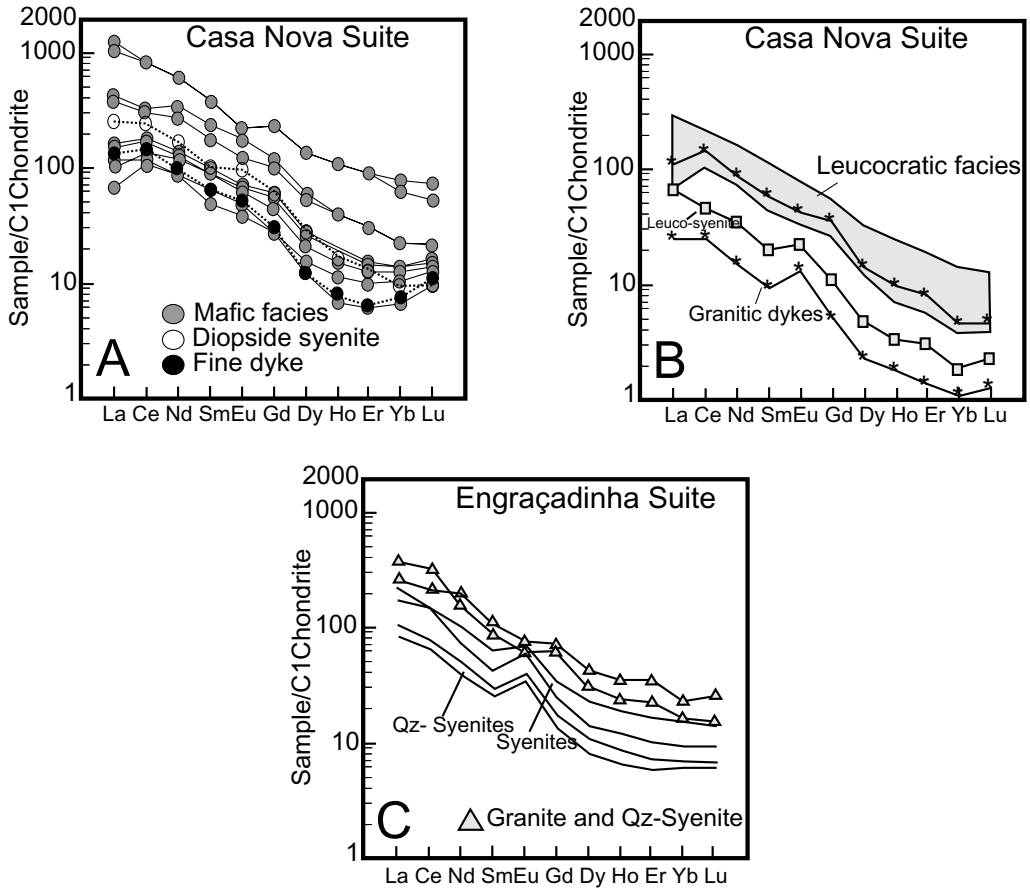

Fig. 12. REE patterns of the RPFB suites, normalised to the chondritic values of Evensen et al. (1978).

Cachoeirinha–Salgueiro Fold Belt (Fig. 10). The spidergrams in Fig. 10 display similar geochemical patterns between these ultrapotassic suites and RPFB rocks.

5.3. Rare earth elements

The chodrite-normalised (C1: Evensen et al., 1978) REE patterns of both suites (Fig. 12), are similar, with a few exceptions.

The ESG have LREE/HREE fractionated patterns, with Ce_N/Yb_N ratios ranging from 9 to 20, increasing from syenites to granites. This variation in the Ce_N/Yb_N ratio is ascribed to apatite and titanite fractionation from syenites to granites. The REE contents reach maximum values in the more differentiated granites and show a relative decrease from less evolved (64 wt% SiO_2) to leucocratic syenites (67 wt% SiO_2). The REE patterns of most syenitic rocks show positive Eu-anomalies, not observed in granites. In the case of syenites, REE patterns are consistent with alkali feldspar cumulative processes, promoting the lack of Eu-anomalies in the granites (Fig. 12).

In contrast to the ESG, the REE patterns in the CNS show compatible behaviour, with a strong and regular decrease in overall REE contents from melanocratic syenites to the more differentiated granitic rocks. The chondrite-normalised REE patterns are roughly parallel, but slight differences may be pointed out. In the melanocratic syenites and in some of the mesocratic ones, the fractionation ratio (Ce_N/Yb_N) is around 20; it shows lower values in the other mafic syenites samples and in the fine-grained mafic dyke, mainly due to HREE enrichment. Syenitic rocks with the lowest total REE contents present REE patterns with "sigmoidal" shape and a well-defined concavity for middle- to heavy-REE (Fig. 12A). This pattern shape is explained by the mineral/melt partition coefficients of REE for apatites and titanites (Green, 1994), assumed to be the major REE carriers in the fractionated phases. These samples also show the lowest TiO_2 and P_2O_5 contents, which is consistent with a strong role for apatite and titanite fractionation in the REE behaviour in these magmas. A similar interpretation supposed for the evolution of leucocratic syenites and granites that have Ce_N/Yb_N ratios around 25 (Fig. 12B).

The melanocratic syenites have small negative Eu-anomalies, probably related to their cumulative origin with alkali feldspar-relative depletion, whereas the granites (Fig. 12B) have positive Eu-anomalies, probably due to the effect of accumulation of alkali feldspar. The diopside-bearing

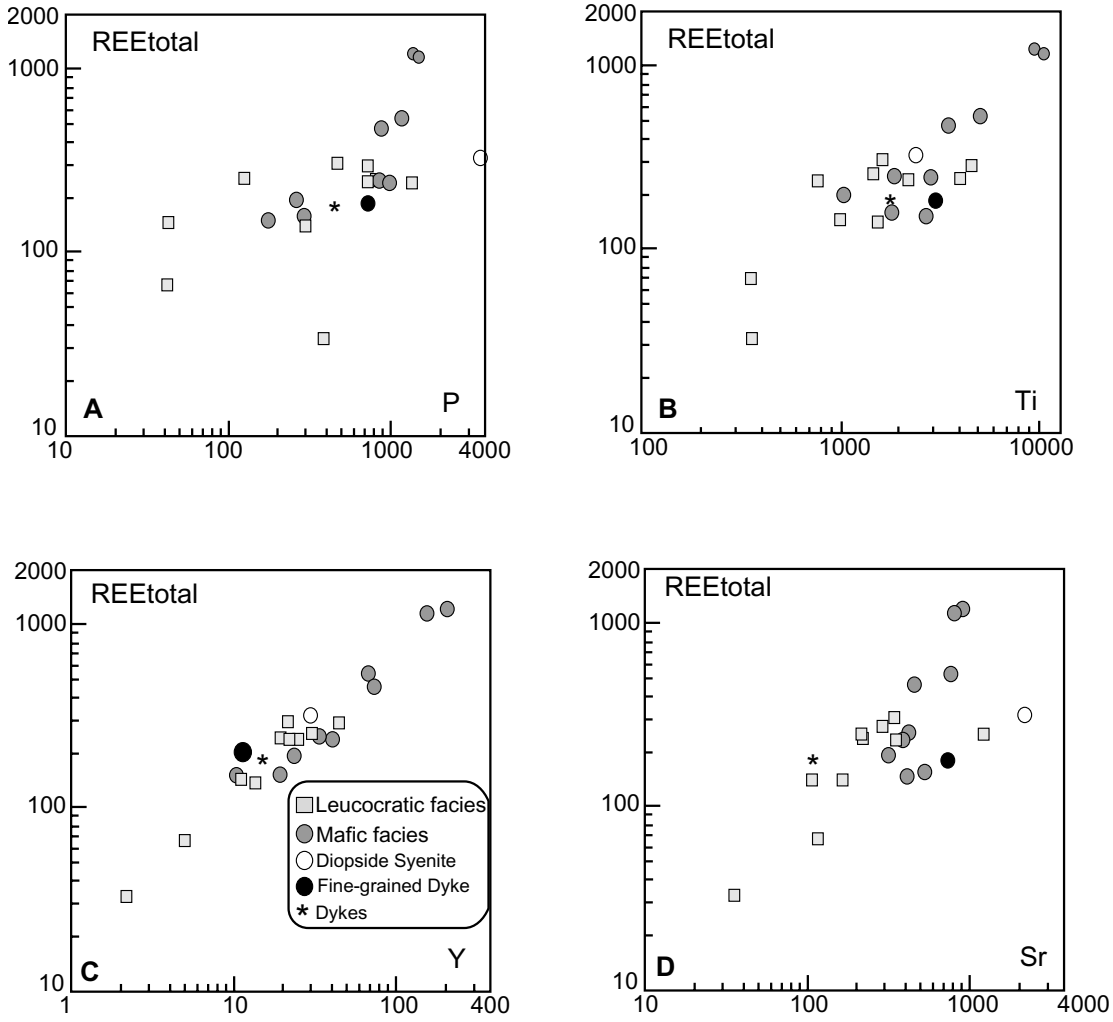

Fig. 13. REE vs. Sr, Y, P, and Ti, showing possible control of these elements by minerals such as apatite and titanite.

syenites have REE patterns intermediate between those of more mafic syenites and those with sigmoidal-type patterns. They have REE patterns with a small positive Eu-anomaly and fractionation ratios ($Ce_N/Yb = 0.7068$) intermediate between those of more mafic syenites and leucocratic syenites.

The compatible behaviour of REE was also observed by Ferreira (1991) in the Triunfo syenites in the CSF. That author attributed this behaviour to the unmixing and immiscibility of two liquids (pyroxenitic and syenitic) during the generation of those syenites. In the RPFB magmatism, the available field relations and whole-rock chemistry are consistent with mineral fractionation processes involving mainly titanite (Plá Cid et al., 1997b) and apatite, and local pyroxene or alkali feldspar accumulations promoted by magmatic flow (Plá Cid et al., 1997b). The positive correlation shown by the total REE contents with Ti, P, Sr, and Y contents (Fig. 13) suggests that the REE behaviour is controlled mainly by crystallisation and flow-segregation of titanite and apatite.

6. Final considerations

Rocks with features typical of those belonging to alkaline, silica-saturated ultrapotassic series frequently occur with associated shoshonites and in a wide range of tectonic settings (Wilson, 1989; Muller et al., 1992). They are observed in within-plate settings (East African Rift), in island arcs (Marianas Arc and Fiji Arc), in active continental margins (Continental Arc, Andes-type), and in post-collisional settings following subduction (Italian Volcanic Province).

Several authors — such as Pearce and Cann (1973), Pearce and Norry (1979), Wood et al. (1979), Pearce (1982), Thompson (1982), Pearce et al. (1984), Briqueau et al. (1984), Sun and McDonough (1989) and Muller et al. (1992) — have tried to correlate the chemical composition of magmatic series with their tectonic setting. Spidergrams of less evolved syenites studied here, normalised to the Ocean Ridge Granite contents (Pearce et al., 1984), show that their low-HFSE contents (Zr, Ta, Nb and Y) rule out an association with within-plate settings. Their contents of Rb

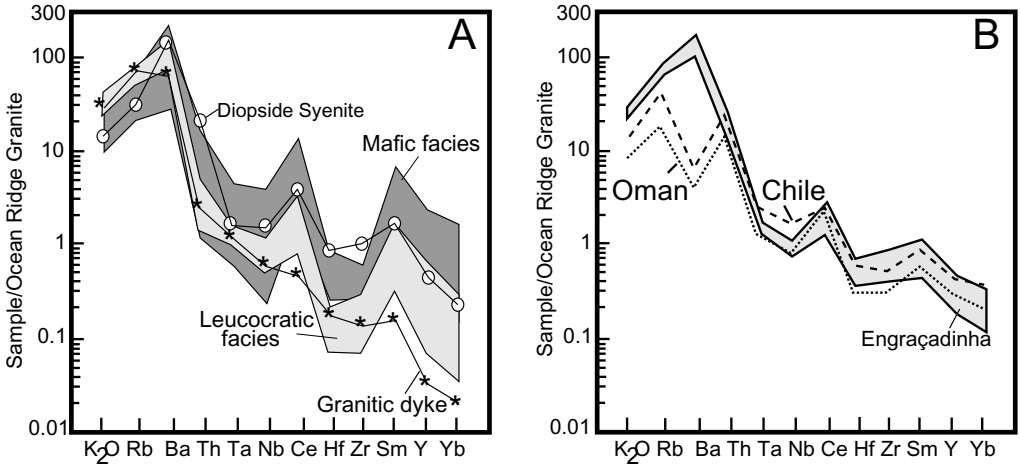

Fig. 14. Spidergrams normalised to the ocean ridge granites (from Pearce et al., 1984) for the RPFB alkaline silica-saturated ultrapotassic suites and typical collisional granites.

and Th, as well as the HFSE previously cited, suggest a mantle lithosphere that was formed in a collisional setting, as exemplified by the collisional granites from Chile or post-collisional from Oman (Fig. 14). The Nb/Ta ratio and Nb values of the RPFB alkaline silica-saturated ultrapotassic rocks are typical of volcanic-arc or collisional magmatism (Green, 1995).

According to the previously described tectono-magmatic models developed for RPFB (Jardim de Sá, 1994), there are strong lines of evidence that point to an arc-related magmatic sequence generated during the Transamazônico Event, but not during the younger Brasiliano Event. Ferreira et al. (1994) proposed also a paleo-subduction zone, probably of Early Proterozoic age, with mantle metasomatism generated by dehydration of an oceanic plate (± sediments), in order to explain the potassium-enriched magmatism represented by the Triunfo syenite in the Cachoerinha–Salgueiro Fold Belt. The high contents in K, LREE, Rb, and Ba, as well as the negative Nb anomalies, are probably inherited from melt of a metasomatised mantle source. The Ta/Yb vs. Th/Yb plot (Fig. 15) show an enriched mantle as a probable source for this magmatism, with values comparable to those found in active continental margin magmatism, such as the ultrapotassic Roman Province. Field relations, isotopic ages (Jardim de Sá, 1994), geochemical signatures, and on models proposed for Salgueiro–Cachoeirinha and Seridó Fold Belts, it is proposed that the RPFB ultrapotassic silica-saturated alkaline rocks were emplaced in the later stages of Brasiliano Collisional Event, and present geochemical characteristics related to a mantle-source modified by a oceanic-plate subduction during the Paleoproterozoic Transamazônico Event.

The suites of the RPFB are related to an ultrapotassic, silica-saturated alkaline magmatism widespread in the northeastern Brazil, mainly in the Cachoeirinha–Salgueiro Fold Belt and rarely observed in other regions of the world.

The ultrapotassic magmatism is accepted as having originated through contamination or fertilisation processes in the mantle during lithosphere subduction (Wyllie and Sekine, 1982). According to Foley and Wheller (1990), this fertilisation is caused by melt contamination rather than by fluids, promoting LILE- and REE-enrichment. In the RPFB rocks, the enrichment is indicated by the high contents of Ba, K, Sr, and LREE, with low concentrations of HFSE. The Sr and P negative anomalies probably result from continuous apatite fractionation during magmatic evolution.

The melanocratic rocks of the CNS probably represent a cumulative process of Na–Ca pyroxene–titanite–apatite during syenite crystallisation, controlled by magmatic-flow segregation. These pyroxenes are aegirine–augite, with acmite-molecular contents similar to or higher than those determined in mesocratic syenites, which indicates approximately the same crystallisation temperature for both lithologies. The compositional gap between mesocratic and melanocratic syenites (Figs. 6 and 8) is another argument for their cumulative origin. The presence of apatite and titanite as the major carriers of REE in the cumulative melanocratic syenites explains the unusual REE patterns, with sigmoidal shape, present in several mesocratic syenites. The diopside-bearing syenites are the most primitive magma of the Casa Nova suite, as suggested by field relations, pyroxene chemistry, and geochemical data, representing a *transsolvus* (Bonin, 1982) syenite. In the LSF, some samples present extreme K_2O contents, which indicates a probable effect of alkali feldspar accumulation. A complete mathematical modelling for these ultrapotassic suites is found in the work reported by Plá Cid et al. (1999b).

The fine-grained mafic dyke is probably a mafic syenitic liquid intruded together with the pegmatitic syenites, presenting a major element composition similar to that of mesocratic syenites. They show a great amount of micro-fractures filled with carbonate, suggesting a CO_2-rich

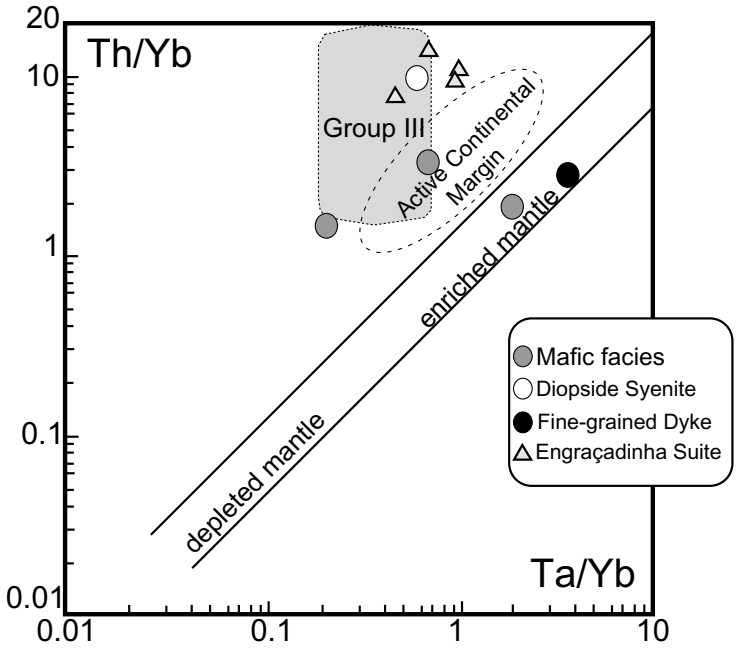

Fig. 15. Th/Yb vs. Ta/Yb diagram (after Wilson, 1989) suggesting an enriched mantle source for the RPFB alkaline ultrapotassic suites.

metasomatism associated with the later stages of the crystallisation of the CNS.

The ESG show Ba–Ti mineralization associated with later magmatic stages. This barite–ilmenite paragenesis is related to a SiO_2 increase, as well as Nb, Th, Sr, and Zr enrichment. The Sr is probably incorporated in barite, Nb in ilmenite, and Th in zircon.

Based upon the field relations, textural features, and geochemical patterns, the Engraçadinha syenites–granites represent a more evolved magmatism, similar to the CNS. This hypothesis is supported by the more evolved composition of aegirine–augite, as well as whole rock chemistry. The magmatic evolution in the Casa Nova alkaline SiO_2-saturated ultrapotassic syenites is controlled by early pyroxene–apatite–titanite cumulative magmatic-flow processes, whereas in the more differentiated Engraçadinha syenites–granites, the evolution was dominated by alkali feldspar cumulative magmatic-flow processes.

The Neoproterozoic RPFB ultrapotassic rocks represent a late-Brasiliano collision-related magmatic event associated with mantle sources modified by a Transamazônico oceanic-plate subduction in a Paleoproterozoic active continental margin setting. This magmatism shows a syenite–granite association, with strong LILE and REE enrichment, and may represent the southwestern prolongation of the Cachoeirinha–Salgueiro megastructure and its syenitic magmatism, as described by Sial (1986), Ferreira (1991) and Da Silva Filho et al. (1993).

Acknowledgements

JPC received financial support from the Fundação Coordenação de Aperfeiçoamento de Pessoal de Nível Superior (CAPES 1772/95-14) and the Conselho Nacional de Pesquisa (CNPq). We are grateful for the assistance of the Centro de Estudos em Petrologia e Geoquímica at UFRGS, the Programa de Pesquisa e Pós-Graduação em Geofísica/PPPG at UFBA, and the Laboratoire de Petrographie et Volcanologie at the Université Paris-Sud XI-Orsay. JPC thanks his wife for her patience.

References

Almeida, F.F.M., Hasui, Y., Brito Neves, B.B., 1977. Províncias Estruturais Brasileiras. Anais do Simpósio de Geologia do Nordeste (Campina Grande, Brasil), pp. 363–391.

Barbosa, J.S.F., Dominguez, J.M.L., 1996. Mapa Geológico do Estado da Bahia, Texto Explicativo. Secretaria da Indústria, Comércio e Mineração do Estado da Bahia, PPPG-Universidade Federal da Bahia, Salvador BA, Brasil, 328 pp.

Bonin, B., 1982. Les Granites des Complexes Annulaires. Manuels et Méthodes, vol. 4, Bureau de Recherches Geologiques et Minieres, Orléans, France, 183 pp.

Briqueau, L., Bougault, H., Joron, J.L., 1984. Quantification of Nb, Ta, Ti and V anomalies in magmas associated with subduction zones: petrogenetic implications. Earth and Planetary Science Letters 68, 297–308.

Brito Neves, B.B., 1975. Regionalização Geotectônica do Pré-Cambriano Nordestino. Tese de Doutorado, Instituto de Geociências, Universidade de São Paulo, São Paulo SP, Brazil, 198 pp.

Bruni, M.A.L., Almeida, J.T., Bruni, E.C., 1974. Texto Explicativo para a Carta Geológica do Brasil ao Milionésimo (Folha Aracaju, SC-24). DNPM, Brasília DF, Brasil, 163 pp.

Caby, R., Arthaud, M., 1987. Petrostructural evolution of the Lagoa Real subalkaline metaplutonic complex (Bahia, Brazil). Revista Brasileira de Geociências 17, 636.

Conceição, H., 1990. Pétrologie du Massif Syénitique d'Itiúba: Contribution à l'Étude Minéralogique des Roches Alcalines dans l'Etat de Bahia

(Brésil). Thèse de Doctorat, Université Paris-Sud XI-Orsay, Paris, France, 395 pp.

Conceição, H., Sabate, P., Bonin, B., 1989. Proterozoic alkaline syenitic massif in Bahia state (Brazil) [abstract]. In: Haapala, I., Kähkönen, Y. (Eds.), Precambrian Granitoids. Geological Survey of Finland, Special Paper, vol. 8, 31 pp.

Conceição, R.V., 1994. Petrologia dos Sienitos Potássicos do Maciço de Santanápolis e alguns Aspectos do Embasamento Granulítico. Dissertação de Mestrado, CPGG-Universidade Federal da Bahia, Salvador BA, Brazil, 275 pp.

Corriveau, L., Heaman, L.M., Marcantonio, F., Van Breeman, O., 1990. 1.1 Ga K-rich alkaline plutonism in the SW Greenville Province: U–Pb constraints for the timing of subduction-related magmatism. Contributions to Mineralogy and Petrology 105, 473–485.

Dalton de Souza, J.A., Fernandes, F.J., Guimarães, J.T., Lopes, J.N., 1979. Projeto Colomi: Geologia da Região do Médio São Francisco, Relatório Final. DNPM/CPRM, Salvador, Brasil.

Da Silva Filho, A.F., Thompson, R.N., Leat, P., 1987. Petrology of the Terra Nova pluton, Brazil, and associated ultrapotassic dykes. Revista Brasileira de Geociências 17, 481–487.

Da Silva Filho, A.F., Guimarães, I.P., Thompson, R.N., 1993. Shoshonitic and ultrapotassic Proterozoic intrusive suites in the Cachoeirinha–Salgueiro belt, NE Brazil: a transition from collisional to post-collisional magmatism. Precambrian Research 62, 323–342.

Dawson, J.B., Smith, J.V., 1977. The MARID (mica-amphibole-rutile-ilmenite-diopside) suite of xenoliths in kimberlite. Geochimica et Cosmochimica Acta 41, 309–322.

Erlank, A.J., Waters, F.G., Hawkesworth, C.J., Haggerty, S.E., Allsopp, H.L., Rickard, R.S., Menzies, M.A., 1987. Evidence for mantle metasomatism in peridotite nodules from the Kimberley pipes, South Africa. In: Menzies, M.A., Hawkesworth, C.J. (Eds.), Mantle Metasomatism. Academic Press, London, pp. 221–311 (472 pp.).

Evensen, N.M., Hamilton, P.J., O'nions, R.K., 1978. Rare earth abundances in chondritic meteorites. Geochimica et Cosmochimica Acta 42, 1199–1212.

Ferreira, V.P., 1991. Petrology and geochemistry of the Late Precambrian ultrapotassic Peralkaline Triunfo Pluton and related Dykes, State of Pernambuco, Northeast Brazil. PhD Thesis, University of Georgia, Athens GA, USA, 269 pp.

Ferreira, V.P., Sial, A.N., Whitney, J.A., 1994. Large scale silicate immiscibility: a possible example from northeast Brazil. Lithos 33, 285–302.

Figuerôa, I., Silva Filho, I., 1990. Geologia da Folha Petrolina. In: Programa de Levantamentos Geológico Básicos do Brasil (PLGBB), Folha SC.24-V-C-III Petrolina, eds DNPM/CPRM, Rio de Janeiro RJ, Brasil, pp. 11–56.

Foley, S.F., 1992. Vein-plus-wall-rock melting mechanisms in the lithosphere and the origin of potassic alkaline magmas. Lithos 28, 435–453.

Foley, S.F., Venturelli, G., Green, D.H., Toscani, L., 1987. The ultrapotassic rocks: characteristics, classification and constraints for the petrogenetic models. Earth Science Reviews 24, 81–134.

Foley, S.F., Wheller, G.E., 1990. Parallels in the origin of the geochemical signatures of island arc volcanics and continental potassic igneous rocks: the role of the residual titanates. Chemical Geology 85, 1–18.

Green, T.H., 1994. Experimental studies of trace-element partitioning applicable to igneous petrogenesis — Sedona 16 years later. Chemical Geology 117, 1–36.

Green, T.H., 1995. Significance of Nb/Ta as an indicator of geochemical processes in the crust-mantle system. Chemical Geology 120, 347–359.

Inda, H.A.V., Barbosa, J.S.F., 1978. Texto Explicativo para o Mapa Geológico do Estado da Bahia. SME/CBPM, Salvador BA, Brasil, 137pp.

Jardim de Sá, E.F., 1994. A Faixa Seridó (Província Borborema, NE do Brasil) e o Seu Significado Geodinâmico na Cadeia Brasiliana/Pan-Africana. Tese de Doutorado, Universidade de Brasília, Brasília DF, Brazil, 795 pp.

Konzett, J., 1997. Phase relations and chemistry of Ti-rich K-richterite-bearing mantle assemblages: an experimental study to 8.0 GPa in a Ti-KNCMASH system. Contributions to Mineralogy and Petrology 128, 385–404.

Laflèche, M.R., Dupuy, C., Dostal, J., 1991. Archean orogenic ultrapotassic magmatism: an example from the southern Abitibi greenstone belt. Precambrian Research 52, 71–96.

Laval, M., Hottin, A.M., 1992. The Mlindi ring structure: an example of an ultrapotassic pyroxenite to syenite differentiated complex. Geologische Rundschau 81 (3), 737–757.

Leite, C.M., 1997. Programa de Levantamentos Geológicos Básicos do Brasil, Folha — SC.23-X-D-IV (Campo Alegre de Lourdes), Escala 1:100000. CBPM/CPRM/SICM, Salvador BA, Brazil, 153 pp.

Le Maitre, R.W., Bateman, P., Dubek, A., Keller, J., Lameyre, J., Le Bas, M.J., Sabine, P.A., Schimid, R., Sorensen, H., 1989. A Classification of Igneous Rocks and Glossary of Terms: Recommendations of the International Union of Geological Sciences Subcommission on the Systematics of Igneous Rocks. Blackwell, Oxford, UK, 193 pp.

Mascarenhas, J.de F., 1979. Evolução geotectônica do Pré-Cambriano do Estado da Bahia. In: Inda, H.A.V. (Ed.), Coordenação de Geologia e Recursos Minerais do Estado da Bahia, vol. 2. SME/CBPM, Salvador BA, Brasil, pp. 57–165.

Middlemost, E.A.K., 1994. Naming materials in the magma/igneous rock system. Earth Science Reviews 37, 215–224.

Mitchell, R.H., 1995. Melting experiments on a sanidine phlogopite lamproite at 4–7 GPa and their bearing on the sources of lamproite magmas. Journal of Petrology 36, 1455–1474.

Mitchell, R.H., Vladykin, N.V., 1996. Compositional variation of pyroxene and mica from the Little Murun ultrapotassic complex, Aldan Shield, Russia. Mineralogical Magazine 60, 907–925.

Muller, D., Rock, N.M.S., Groves, D.I., 1992. Geochemical discrimination between shoshonitic and potassic volcanic rocks in different tectonic settings: a pilot study. Mineralogy and Petrology 46, 259–289.

Oyawoye, M.O., 1976. The origin and evolution of the potassic rocks of SW Nigeria. Abstracts of the XXIX International Geological Congress 21 (10A), 424–425.

Pearce, J.A., 1982. Trace element characteristics of lavas from destructive plate boundaries. In: Thorpe, R.S. (Ed.), Andesites, Orogenic Andesites and Related Rocks. Wiley, Chichester, UK, pp. 525–548 (724 pp.).

Pearce, J.A., 1983. Role of the sub-continental lithosphere in magma genesis at active plate margins. In: Hawkesworth, C.J., Norry, M. (Eds.), Continental Basalts and Mantle Xenoliths. Shiva Publishing, Nantwich, UK, pp. 230–249 (272 pp.).

Pearce, J.A., Cann, J.R., 1973. Tectonic setting of basic volcanic rocks investigated using trace element analyses. Earth and Planetary Science Letters 19, 290–300.

Pearce, J.A., Norry, M.J., 1979. Petrogenetic implications of Ti, Zr, Y and Nb variation in volcanic rocks. Contributions to Mineralogy and Petrology 69, 33–47.

Pearce, J.A., Harris, N.B.W., Tindle, A.G., 1984. Trace element discrimination diagrams for the tectonic interpretation of granitic rocks. Journal of Petrology 25, 956–983.

Plá Cid, J., Nardi, L.V.S., Conceiçã, H., Bonin, B., 1997a. O magmatismo alcalino da faixa de dobramentos Riacho do Pontal e da borda noroeste do Cráton do São Francisco, norte do Estado da Bahia, Brasil: Uma síntese. Actas da X Semana de Geoquímica e IV Congresso de Geoquímica dos Países de Língua Portuguesa, Braga, Portugal, pp. 127–130.

Plá Cid, J., Nardi, L.V.S., Conceiçã, H., Bonin, B., 1997b. Alkalic plutonic activity within in the Riacho do Pontal fold belt, NE Brazil. Second International Symposium of Granites and Associated Mineralizations, Salvador, Brazil, Extended Abstracts and Program, pp. 143–144.

Plá Cid, J., Nardi, L.V.S., Conceiçã, H., 1999a. Critérios mineralógicos e geoquímicos para a classificação do magmatismo alcalino saturado em sílica: o exemplo com sienitos do Brasil. I Simpósio sobre Vulcanismo e Ambientes Associados, Gramado RS, Brasil, Boletim de Resumos, p. 28.

Plá Cid, J., Nardi, L.V.S., Conceiçã, H., Bonin, B., 1999b. Petrogenesis of

the Neoproterozoic alkaline ultrapotassic suites of northeastern Brazil: major- and trace-element evidence from pyroxene chemistry and numerical modeling. International Geology Review 41 (11), 1005–1028.

Pognante, U., 1990. Shoshonitic and ultrapotassic post-collisional dykes from northern Karakorum (Sinkiang, China). Lithos 26, 305–316.

Rocha, G.M.F., 1991. Projeto Distrito Manganesífero do Sudoeste da Bahia. Comércio e Turismo/Superintendência de Geologia e Recursos Minerais, Secretaria de Industria, Salvador RS, Brazil, 107 pp.

Rosa, M.L.S., 1994. Magmatismo Shoshonítico e Ultrapotássico no Sul do Cinturão Móvel Salvador-Curaça, Maciço de São Félix: Geologia, Mineralogia e Geoquímica. Dissertação de Mestrado, CPGG, Instituto de Geociências, Universidade Federal da Bahia, Salvador BA, Brazil, 241 pp.

Santos, E.J., Caldasso, A.L.S., 1978. Síntese dos conhecimentos e ensaio interpretativo da área do Riacho do Pontal, Nordeste do Brasil. In: Rocha, A.J.D., Misi, A., Torquato, J.R.F., Lima, O.A.L., Costa, P.H.O. (Eds.), Anais da Reunião Preparatória para o Simpósio sobre o Cráton do São Francisco e Suas Faixas Marginais. Publicações Especiais, Salvador BA, Brazil, pp. 399–433 (SBG/NBA-SE).

Schobbenhaus, C., Campos, D.A., Derze, G.R., Asmus, H.E., 1984. Geologia do Brasil: Texto Explicativo do Mapa Geológico do Brasil e da Área Oceânica Adjacente Incluindo Depósitos Minerais, Escala 1: 2 500 000. Departamento Nacional de Produção Mineral (DNPM). Brasília DF, Brasil, 501 pp.

Sial, A.N., 1986. Granitic types in northeast Brazil: current knowledge. Revista Brasileira de Geociências 16 (1), 54–72.

Sial, A.N., Ferreira, V.P., 1988. Brasiliano age peralkaline plutonic rocks of the Central Structural Domain, northeast Brazil. Rendiconti della Societa Italiana di Mineralogia e Petrologia 43 (2), 307–342.

Silva, M.E., 1987. O Sistema de Dobramentos Rio Preto e Suas Relações com o Cráton do São Francisco. Dissertação de Mestrado, Instituto de Geociências, Universidade de Brasília, Brasília DF, Brazil, 143 pp.

Smith, I.E., 1972. High potassium intrusives from southeastern Papua. Contributions to Mineralogy and Petrology 34, 167–176.

Streckeisen, A., 1976. To each plutonic rock its proper name. Earth Science Reviews 12, 1–33.

Sun, S.S., McDonough, W.F., 1989. Chemical and isotopic systematics of oceanic basalts: Implications for mantle composition and processes. In: Saunders, A.D., Norry, M.J. (Eds.), Magmatism in the Ocean Basins. Geological Society of London, Special Publication, vol. 42, pp. 313–345.

Thompson, R.N., 1982. Magmatism of the British Tertiary volcanic province. Scottish Journal of Geology 18, 50–107.

Thompson, R.N., Dickin, A.P., Gibson, I.L., Morrison, M.A., 1982. Elemental fingerprints of isotopic contamination of Hebridean Paleocene mantle-derived magmas by Archean sial. Contributions to Mineralogy and Petrology 79, 159–168.

Thompson, R.N., Fowler, M.B., 1986. Subduction-related shoshonitic and ultrapotassic magmatism: a study of Siluro–Ordovician syenites from the Scottish Caledonides. Contributions to Mineralogy and Petrology 103, 470–492.

Wernick, E., 1981. The Archean of Brazil. Earth Science Reviews 17, 31–48.

Wilson, M., 1989. Igneous Petrogenesis: A Global Tectonic Approach. Unwin & Hyman, London, UK, 466 pp.

Wood, D.A., Joron, J.L., Treuil, M., 1979. A re-appraisal of the use of trace elements to classify and discriminate between magma series erupted in different tectonic settings. Earth and Planetary Science Letters 45, 326–336.

Wyllie, P.J., Sekine, T., 1982. The formation of phlogopite in subduction zone hybridization. Contributions to Mineralogy and Petrology 79 (4), 375–380.